AD-A142 433 PROPAGATION LOSS IN ELECTROSTATICALLY VARIABLE SAW DELAY LINES(U) ROME AIR DEVELOPMENT CENTER GRIFFISS AFB NY H L BERTONI FEB 84 RADC-TR-84-6 1/1

UNCLASSIFIED F/G 9/1 NL

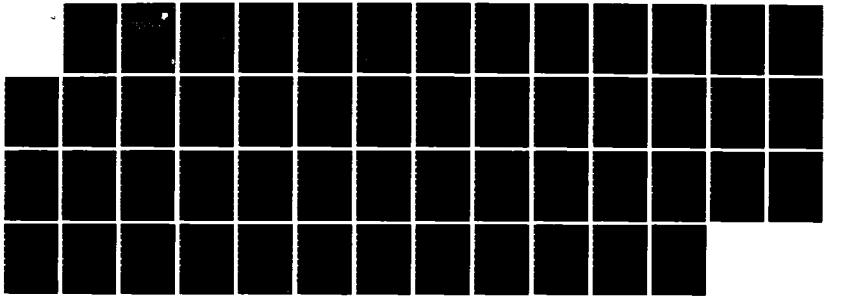

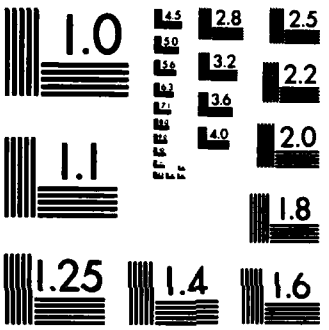

(12)

RADC-TR-84-6
In-House Report
February 1984

PROPAGATION LOSS IN ELECTROSTATICALLY VARIABLE SAW DELAY LINES

Henry L. Bertoni (USAF/AFOSR)

ROME AIR DEVELOPMENT CENTER
Air Force Systems Command
Griffiss Air Force Base, NY 13441

This report has been reviewed by the RADC Public Affairs Office (PA) and is releasable to the National Technical Information Service (NTIS). At NTIS it will be releasable to the general public, including foreign nations.

RADC-TR-84-6 has been reviewed and is approved for publication.

APPROVED: John K. Schindler

JOHN K. SCHINDLER
Chief, Antennas & RF Components Branch
Electromagnetic Sciences Division

APPROVED: Allan C. Schell

ALLAN C. SCHELL
Chief, Electromagnetic Sciences Division

FOR THE COMMANDER: John A. Ritz

JOHN A. RITZ
Acting Chief, Plans Office

If your address has changed or if you wish to be removed from the RADC mailing list, or if the addressee is no longer employed by your organization, please notify RADC (EEAC) Hanscom AFB MA 01731. This will assist us in maintaining a current mailing list.

Do not return copies of this report unless contractual obligations or notices on a specific document requires that it be returned.

Unclassified

SECURITY CLASSIFICATION OF THIS PAGE (When Data Entered)

REPORT DOCUMENTATION PAGE	READ INSTRUCTIONS BEFORE COMPLETING FORM
1. REPORT NUMBER: RADC-TR-84-6	2. GOVT ACCESSION NO.: AD-A142 433
	3. RECIPIENT'S CATALOG NUMBER
4. TITLE (and Subtitle): PROPAGATION LOSS IN ELECTROSTATICALLY VARIABLE SAW DELAY LINES	5. TYPE OF REPORT & PERIOD COVERED: In-House
	6. PERFORMING ORG. REPORT NUMBER
7. AUTHOR(s): Henry L. Bertoni(USAF/AFOSR)	8. CONTRACT OR GRANT NUMBER(s)
9. PERFORMING ORGANIZATION NAME AND ADDRESS: Rome Air Development Center (EEAC) Hanscom AFB Massachusetts 01731	10. PROGRAM ELEMENT PROJECT TASK AREA & WORK UNIT NUMBERS: 61102F 2305J501
11. CONTROLLING OFFICE NAME AND ADDRESS: Rome Air Development Center (EEAC) Hanscom AFB Massachusetts 01731	12. REPORT DATE: February 1984
	13. NUMBER OF PAGES: 51
14. MONITORING AGENCY NAME & ADDRESS(if different from Controlling Office)	15. SECURITY CLASS. (of this report): Unclassified
	15a. DECLASSIFICATION DOWNGRADING SCHEDULE

16. DISTRIBUTION STATEMENT (of this Report)

Approved for public release; distribution unlimited.

17. DISTRIBUTION ST ENT (of abstract entered in Block 20, if different from Report)

18. SUPPLEMENTARY TES

Prof. Henry L. Bertoni performed this research as an AFOSR Summer Faculty Fellow at RADC/EEAC. His permanent address is Polytechnic Institute of New York, 333 Jay Street, Brooklyn, N.Y. 11201.

19. KEY WORDS (Continue on reverse side if necessary and identify by block number)

Surface Acoustic Wave (SAW)
Time delay unit
Electronically variable delay line

20. ABSTRACT (Continue on reverse side if necessary and identify by block number)

Variations in SAW time delay due to an applied dc electric field has been suggested as a means for achieving the phase shift needed for each radiating element in phased-array antennas. Important device parameters are: (1) insertion loss and, (2) sensitivity of delay change to dc terminal voltage. These parameters can be in competition, in that device modifications intended to improve one parameter may make the other worse. These parameters are considered for the normal-field configuration, and for the in-plane .

DD FORM 1 JAN 73 1473

Unclassified

SECURITY CLASSIFICATION OF THIS PAGE (When Data Entered)

20. Abstract (Contd)

configuration in which both dc electrodes are on the same surface as the SAW. The in-plane configuration can have high-voltage sensitivity if the electrodes are close together, but diffraction loss for this case is found to be large for long path lengths. Methods for limiting diffraction loss without reducing voltage sensitivity are investigated.

Preface

The author wishes to thank Alan J. Budreau and Paul H. Carr for suggesting the topic of this report and for sharing their ideas and experimental results. The author also wishes to thank Andrew J. Slobodnik, Jr. and Jose H. Silva for their support and technical discussions. The financial support of the Air Force Systems Command, Air Force Office of Scientific Research, and the Rome Air Development Center is gratefully acknowledged.

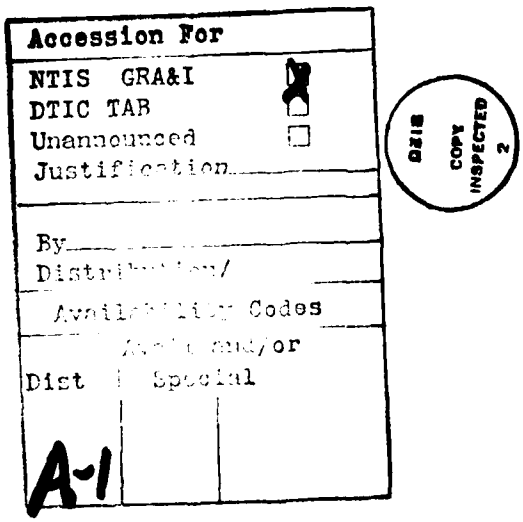

Contents

Illustrations

Propagation Loss in Electrostatically Variable SAW Delay Lines

1. INTRODUCTION

Phase shifters are currently used in steering the beam in phased array antennas. Electronically variable time-delay lines rather than phase shifters are required for wide instantaneous bandwidths. It has been found that strong dc electric fields change the time delay in surface acoustic wave (SAW) devices.[1-3] This effect has the potential for providing time delay from inexpensive devices fabricated by photolithographic techniques.

The first configuration of dc electrodes to be studied[1, 2] employed an electric field normal to surface on which the SAW propagates. The field was generated by a voltage applied to a metallic film deposited on the surface. Because of the thickness of the piezoelectric crystal plate needed for mechanical strength, rather high terminal voltages were needed to achieve significant velocity change.

(Received for publication 25 January 1984)

1. Joshi, S.G., and Dasgupta, B.B. (1981) Electronically variable surface acoustic wave time delay using a biasing electric field, Proc. 1981 IEEE Ultrasonics Symp., pp. 319-323.

2. Joshi, S.G. (1982) A temperature compensated high voltage probe using surface acoustic waves, Proc. 1982 IEEE Ultrasonics Symp., pp. 317-320.

3. Budreau, A.J., Carr, P.H., and Silva, J.H. (1982) New configuration for electronically variable SAW delay line, Proc. 1982 IEEE Ultrasonics Symp., pp. 399-400.

Budreau, et al[3] proposed the in-plane configuration, in which dc voltage is applied between two electrodes, both deposited on the SAW surface and lying on either side of the propagation region. Because the electrode gap can be made much less than the plate thickness, this configuration can have higher velocity sensitivity to dc terminal voltage. For convenience in fabrication the electrodes were in the form of bars approximately 50-SAW wavelengths wide.

As a result of attenuation in the metal film, the electrodes affect the SAW propagation as if they were semi-infinite. Shorting of the RF electric field by the electrodes slows the SAW propagating beneath them. Thus, the SAW propagates from input to output transducer in a high velocity channel or gap between two semi-infinite regions of low velocity. This arrangement is opposite to that known to act as a waveguide,[4, 5] For the long paths needed to achieve voltage sensitivity, the high velocity gap may have large diffraction loss. This loss is expected to increase with decreasing gap width.

2. OBJECTIVES OF THE RESEARCH EFFORT

The purpose of this study is to investigate the tradeoffs between propagation loss and voltage sensitivity, and to seek improvements that can be achieved by modification of the electrode geometry. Transducer bandwidth requirements strongly favor the high coupling cuts of $LiNbO_3$, for which the relation between velocity change and electrostatic field has been obtained experimentally. For this reason, we do not consider improvements in voltage sensitivity that might result from using other materials.

Consideration is first given to the normal field configuration. It is shown that raising the electrode slightly off the surface reduces SAW attenuation. However, voltage sensitivity is decreased.

Diffraction loss for the in-plane configuration is then investigated. Scalar wave theory is used to represent the 2-D SAW propagation. An expression is derived for the diffraction loss due to wide electrodes. This expression confirms the expectation of high loss for long, narrow gaps.

Two methods for reducing diffraction loss are considered. One method employs electrodes whose width is one half of an appropriately defined wavelength. To first order, these electrodes are invisible to the SAW, so that the diffraction loss is nearly that of a free surface.

---

4. Schmidt, R.U., and Coldren, L.A. (1975) Thin film acoustic surface waveguides on anisotropic media, IEEE Trans. SU-22:115-122.

5. Tiersten, H.F. (1969) Elastic surface waves guided by thin films, J. Appl. Phys. 40:770-789.

Another method considered to reduce diffraction loss employs an overlay of acoustically fast material deposited on top of the electrodes. For sufficiently thick overlay, the SAW under the electrodes becomes fast as compared to the gap region, so that the configuration acts as a slot waveguide.[4, 5] This case involves a mode coupling loss that is independent of gap length, rather than diffraction loss.

3. BASIC DEVICE CONSIDERATIONS

The performance of electrostatically varied delay lines involves three factors: dispersion, insertion loss, and voltage sensitivity. Of the three, dispersion appears to be the least significant for application to phased array radar, since serious degradation of the antenna performance occurs only for velocity changes greater than about 10 percent over the operating band. Insertion loss and voltage sensitivity are critical factors, and changing device parameters to improve one factor frequently makes the other worse. The size of the three factors, and some suggestions for improvement are discussed below for both the normal-field and in-plane configurations.

3.1 Normal-Field Configuration

The normal-field configuration is shown in Figure 1, including a modified electrode configuration. This modification employs a top electrode separated from the surface of the piezoelectric crystal by a distance H. In the usual device, the top electrode consists of a plating of thickness h deposited directly on the crystal surface (H = 0).

3.1.1 DISPERSION

For thin platings, dispersion is proportional to ωh, where ω is the radian frequency ($\omega = 2\pi f$), as discussed in Reference 6. A conducting plating can slow the Rayleigh wave as a result of mass loading, over and above the slowing due to shorting of the piezoelectric field. The slowing due to mass loading by a 600 Å thick Al plating on $LiNbO_3$ is given by

$$\frac{\Delta V}{V_R} = \begin{cases} \left(\frac{f}{f_o}\right) 2.03 \times 10^{-3} & (16\text{-}1\ 2^\circ \text{ doubly rotated}) \\ \left(\frac{f}{f_o}\right) 3.142 \times 10^{-3} & (37^\circ - X)\ , \end{cases} \tag{1}$$

6. Auld, B.A. (1973) Acoustic Fields and Waves in Solids, Vol. II, Wiley and Sons, New York, pp. 274-278.

where f_o = 1 GHz. It is seen that even for a 1-GHz bandwidth the dispersion is only a few tenths of a percent, and hence not significant for radar applications. For the raised electrode configuration (H ≠ 0), no dispersion will occur.

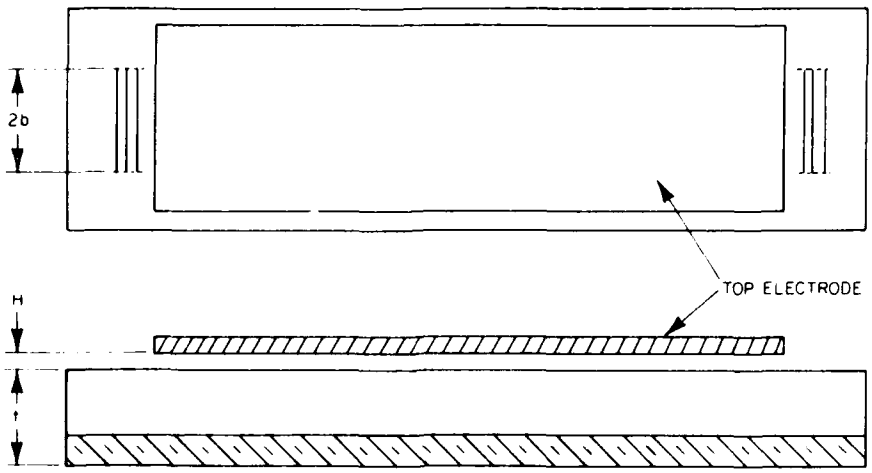

Figure 1. Top and Side Views of the Normal-field Electrode Configuration

3.1.2 INSERTION LOSS

Insertion loss for the normal-field configuration consists of the transducer and diffraction loss found in any delay line, plus the loss in the plating for the case H = 0. This configuration places no special limit on the aperture 2b of the interdigital transducers, so that diffraction loss can be made small by choosing the aperture large enough.

The presence of a film deposited on the crystal will cause loss that is approximately proportional to f^2. Using a laser probe Davis and Weller[7] measured attenuation for frequencies in the range 270 to 730 MHz for Al films 500, 1000, and 2000 Å thick on YZ $LiNbO_3$. Their data for the best films approximately fits the expression

$$\alpha = 9.5 \left(\frac{f}{f_o}\right)^{2.2} \left(\frac{h}{600}\right)^{0.4} \text{ dB/cm} \quad , \tag{2}$$

7. Davis, K. L., and Weller, J. F. (1979) SAW attenuation in metal film - coated delay lines, Proc. 1979 IEEE Ultrasonics Symp., pp. 659-662.

where h is in Angstroms and f_o = 1 GHz. For comparison, the free surface attenuation on $LiNbO_3$ is given in Reference 8 as

$$\alpha = 2.5\left(\frac{f}{f_o}\right)^2 + 0.54\left(\frac{f}{f_o}\right) \text{ dB/cm} \quad . \tag{3}$$

Thus, at f = 1 GHz, a good quality film of thickness 600 Å increases the attenuation by 6.5 dB/cm.

Using the concept of viscosity of the electron gas in metal films, Snider, et al[9] have computed the attenuation due to thin Al films on $LiNbO_3$. For kh small, the attenuation is proportional to $\omega^2 h$. Scaling their calculations at 2-GHz leads to the expression

$$\alpha = 13.2\left(\frac{f}{f_o}\right)^2 \left(\frac{h}{600}\right) \text{ dB/cm} \quad . \tag{4}$$

This attenuation is somewhat greater than the measurements[7] and has a different power dependence on h. Their calculations do not include loss in the $LiNbO_3$ crystal or dissipation in the film due to currents generated by the electric field. In spite of these differences, (2) and (4) give roughly the same attenuation for 600 Å thick films.

Lifting the top electrode off the surface (H ≠ 0) eliminates the loss due to mechanical vibration of the electrode material. For H greater than about a Rayleigh wavelength, the currents induced in the electrode, and hence dissipation, will be negligible. However, this reduction in loss will be accompanied by a reduction in sensitivity, as discussed below.

3.1.3 VOLTAGE SENSITIVITY

Assume that the change in SAW velocity is due to the electrostatic bias field E_o present within the crystal. Then, lifting the electrode off the surface will reduce E_o, and hence reduce the change in velocity per applied Volt. Since $E_o = V_{DC}/(t + \varepsilon H)$, where V_{DC} is the applied voltage and ε is the relative dielectric constant normal to the plate, lifting the electrode off the surface reduces the voltage sensitivity by the factor

---

8. Slobodnik, A.J., Jr., Carr, P.H., and Budreau, A.J. (1970) Microwave frequency acoustic surface-wave loss mechanisms on $LiNbO_3$, J. Appl. Phys. 41:4380-4387.

9. Snider, D.R., Fredricksen, H.P., and Schneider, S.C. (1981) Surface acoustic wave attenuation by a thin film, J. Appl. Phys. 52:3215-3222.

$$\frac{t}{t + \varepsilon H} = \frac{1}{1 + \varepsilon H/t} \quad . \tag{5}$$

If H = 5 μm and t = 10 mill = 250 μm, then using $\varepsilon = \varepsilon^{T}_{xx} = 84$ for $LiNbO_3$ gives the value 0.37 for the Factor (5), while a gap H = 10 μm gives the value 0.23.

3.2 In-Plane Field Configuration

The in-plane configuration shown in Figure 2 allows the dc bias electrodes to be moved closer together in order to improve voltage sensitivity and to avoid the dispersion and loss associated with the deposited film of normal-field configuration.[3] If 2b ≤ 2a, then the film does not lie in the SAW path, and hence does not cause dispersion. However, the film does increase diffraction loss, which may become large as the acoustic aperture 2b is made small. Diffraction loss is considered after a preliminary discussion of the effects of geometry on the voltage sensitivity.

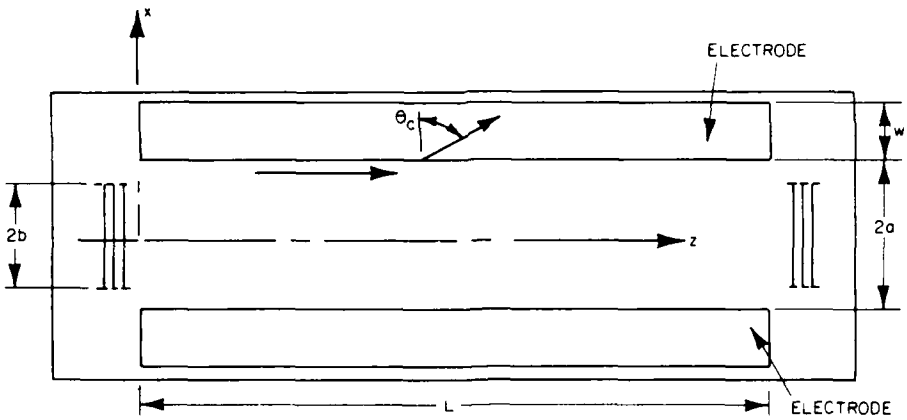

Figure 2. Top View of the Electrodes for the In-plane Field Configuration

3.2.1 GEOMETRICAL EFFECTS

The electric field between the electrodes is shown end-on in Figure 3. Because the dc electric field is transverse to the saggital plane; it will affect the SAW velocity through a different combination of crystal constants than in the normal-field configuration. The significance of this change in orientation has not yet been studied.

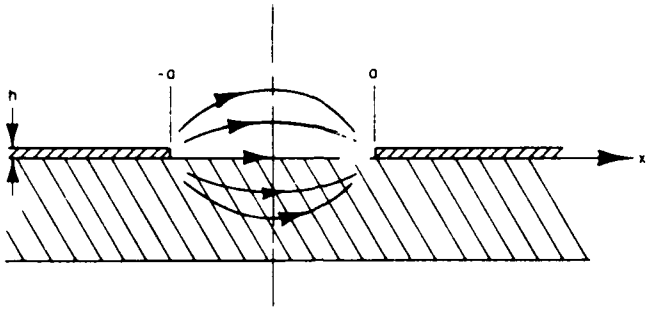

Figure 3. End View of the In-plane Field Configuration Showing the Fringing Static Electric Field

In addition to the orientation effect, the geometry of Figure 3 will influence the voltage sensitivity through the variation of E_x over the range $-a < x < a$. A simple expression for E_x along the crystal surface is obtained from the solution for zero thickness electrodes that are semi-infinite in x, and assuming the principal axes of the crystal to be oriented along the coordinate axes of Figure 3. With these approximations one has[10]

$$E_x = \left(\frac{V_{DC}}{\pi a}\right) \frac{1}{\sqrt{1 - (x/a)^2}} \quad . \tag{6}$$

For electrodes of finite thickness h, (6) is not valid for a-x less than about h, and E_x remains finite as $x \to a$.

The effect of the spatial variation of $\underline{E}$ can be understood from Figure 2. Suppose that the transducer width 2b is sufficiently large (or L is sufficiently small) so that SAW propagation may be taken as being parallel to the z axis. For each value of x, the SAW velocity $V_R(x)$ will be different due to the non-uniformity of E_x. Thus, the phase of the SAW at the output transducer will depend on x. For small changes in velocity, the phase variation with x is given by

$$\phi(x) = \frac{\omega L}{V_R(x)} \approx \left(\frac{\omega L}{V_R}\right) \left[1 - \frac{\Delta V(x)}{V_R}\right] \quad .$$

10. Durand, E. (1953) Electrostatique et Magnetostatique, Masson, Paris, pp. 302-303.

where V_R is the free-surface Rayleigh velocity. If A(x) is the SAW amplitude distribution at the output transducer, the output voltage V_{RF} will be proportional to

$$V_{RF} \propto e^{ik_1 L} \int_{-b}^{b} \left[A(x)\, e^{-ik_1 L \Delta V(x)/V_R} \right] dx \quad , \tag{7}$$

where

$$k_1 = \omega / V_R \quad . \tag{8}$$

Assuming that $\Delta V(x)$ is proportional to E_x of (6), then $\Delta V / V_R$ can be written

$$\frac{\Delta V(x)}{V_R} = \gamma \frac{V_{DC}}{2a} \frac{2}{\pi} \frac{1}{\sqrt{1 - (x/a)^2}} \quad , \tag{9}$$

where γ is a phenomenological sensitivity parameter. Expression (9) is symmetric in x, so that assuming A(x) is also symmetric, (7) reduces to

$$V_{RF} \propto 2 e^{ik_1 L} \int_{0}^{b} A(x) \exp \left[-ik_1 L \frac{\Delta V(0)}{V_R} \frac{1}{\sqrt{1 - (a/x)^2}} \right] dx \quad , \tag{10}$$

where

$$\frac{\Delta V(0)}{V_R} = \gamma \frac{V_{DC}}{2a} \frac{2}{\pi} \tag{11}$$

is the change of velocity along the centerline of the device.

The change in velocity is obtained experimentally by measuring the change in phase of the output voltage with applied dc bias voltage. As seen from (10), the change of output phase in fact represents a weighted average of the change in velocity. Two aspects of the integrand make the central portion of gap between the dc electrodes more important in the weighting than the region near the electrodes ($x \to a$). The first aspect relates to the variation of A(x), while the second relates to the rapid phase variation as $x \to a$.

In general, A(x) will decrease as the ends of the transducer are approached. For $a > b$, as in Figure 2, the integration does not even approach the edges $x = a$ of the dc electrode. Even if $a = b$ and A(a) is not small, the rapid variation of

phase in the exponential as $x \to a$ will cause the integration over neighboring half periods to cancel. The primary contribution to (10) comes from a range of $x < a$ for which $1/\sqrt{1 - (x/a)^2} \approx 1$. Thus, we may approximate (10) as

$$V_{RF} \propto 2e^{ik_1 L} e^{-ik_1 \Delta V(0)/V_R} \int_0^b A(x)\, dx \quad . \tag{12}$$

Expression (12) indicates that the apparent velocity change is approximately the value $\Delta V(0)$ along the centerline. Thus, the electrode geometry reduces the voltage sensitivity by $2/\pi$ as compared to that of parallel plane electrodes having the same spacing.

To test the foregoing model, we have plotted the variation of $\Delta V(0)/V_R$ in (11) with gap width 2a in Figure 4 superimposed on measured values of sensitivity ($\Delta V/V_R$ per Volt) reported by Budreau et al.[11] The amplitude of the computed curve has been normalized so as to pass through the measured point at $2a = 40\ \mu m$. The agreement with the measured variation is quite good considering the simplicity of the model.

In the actual devices measured, the transducer aperture 2b was greater than the separation 2a between the electrodes. The SAW fields propagating beneath the electrodes would not be affected by the dc field in the gap. If these SAW fields reached the output transducer they would affect the phase of the output voltage, and hence, the apparent SAW velocity. The accuracy of the simple model discussed above suggests that these fields do not reach the output transducer, probably because of attenuation due to the film. Consistent with SAW attenuation under the film, the normal component of dc field between the electrodes and the ground plane at the bottom of the crystal plate does not seem to have significantly influenced the measured SAW velocity.

The largest changes in velocity reported in Reference 3 for the in-plane configuration was about $\Delta V/V_R \approx 2 \times 10^{-5}$ for L = 14 mm at a frequency of 900 MHz. For these values, the phase changes along the centerline due to applied dc voltage is $k_1 L \Delta V/V_R \approx (0.006)2\pi$. Because the phase change is so small, the variation of phase with x across the aperture will be less than π, except for $x \to a$. As a result, little phase cancellation will occur in the integral of (10). Had the phase change along the centerline been close to 2π, then significant phase cancellation would result in the integration, and one would expect to see marked variations in the amplitude of the rf output voltage with applied dc voltage, and possibly phase reversals.

11. Budreau, A.J., Carr, P.H., and Bertoni, H.L. (1983) Highest sensitivity electrically variable SAW delay line, Proc. 1983 IEEE Ultrasonics Symp.

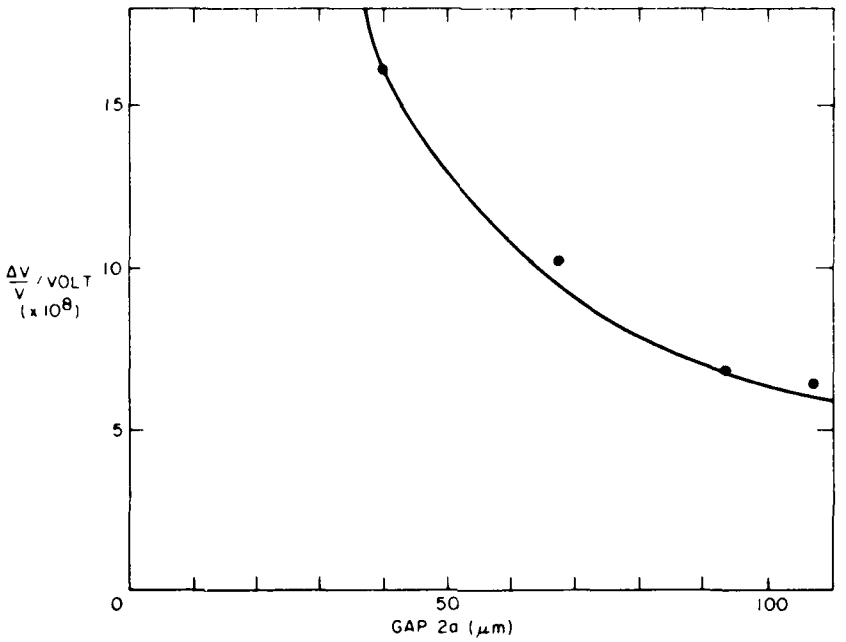

Figure 4. Variation of Voltage Sensitivity With Electrode Gap for the In-plane Field Configuration. Measured points are taken from Reference 11 for the 37-X cut of $LiNbO_3$

In the next section we discuss insertion loss due to diffraction. It is shown that this loss can be reduced by using narrow dc electrodes. The model described above indicates that width of the electrodes does not affect sensitivity, so that some improvement in loss is possible without sacrificing sensitivity.

3.2.2 DIFFRACTION LOSS

The dc electrodes shown in Figure 2 for the in-plane configuration slow the SAW propagating beneath them due to piezoelectric shorting and mass loading. Because of the slowing, waves propagating parallel to the edge of the electrode in the free surface region will be refracted at a finite angle θ_c into the electrode region, as shown in Figure 2. As a result of this refraction, less energy will reach the output transducer, and hence path loss will increase.

An integral expression for the diffraction loss due to wide dc electrodes is derived in Appendix A. Because the fields propagating beneath the electrodes for the case when the transducer aperture (2b) is greater than electrode spacing (2a) do not seem to contribute to the output, we have treated the simpler case, $2a \geq 2b$. Using Fourier transform techniques and deforming the path of

integration, it is found that for electrode spacing wide compared to SAW wavelength, the diffraction loss D_L between the transducers is given by the factor

$$D_L = \frac{2b}{\pi} \int_0^\infty \left(\frac{\sin \eta_1 b}{\eta_1 b} \right)^2 e^{i(\kappa - k_1)L} f(\eta_1)\, d\eta_1 \quad . \tag{13}$$

where

$$f(\eta_1) = \frac{\eta_1 \eta_2}{\eta_1^2 + (\eta_2^2 - \eta_1^2) \cos^2 \eta_1 a} \quad . \tag{14}$$

In these expressions η_1 and κ are the wave numbers along x and z, respectively, of a SAW propagating on the free surface of the piezoelectric crystal. For the same wave number κ along z, a SAW propagating in the electroded region has wave number η_2 along x. Thus, κ and η_2 may be regarded as functions of η_1. Finally, k_1 is the free surface SAW wave number for a wave propagating in the z direction. In the parabolic approximation,

$$\left.\begin{aligned} \kappa &= \sqrt{k_1^2 - \alpha_1^2 \eta_1^2} \\ \eta_2 &= \frac{1}{\alpha_2} \sqrt{\left(k_2^2 - k_1^2\right) + \alpha_1^2 \eta_1^2} \end{aligned}\right\} \quad . \tag{15}$$

Here k_2 is the plated surface SAW wave number for a wave propagating along z and α_i (i = 1, 2) is related to the anisotropy parameter $\gamma = d^2V(\theta)/d\theta^2$ of Reference 12 via

$$\alpha_i^2 = 1 + \gamma_i \quad . \tag{16}$$

In the case when $\eta_1 = \eta_2$, so that SAW propagation on the plated surface is the same as the free surface, it is seen from (14) that $f(\eta_1) = 1$. For this condition (13) reduces to the ordinary diffraction loss between two uniform IDT's. If $\eta_2^2 - \eta_1^2 \ll \eta_1^2$, it is argued in Appendix A that for $a \gg b$, (13) reduces to the value obtain for a free surface, as is to be expected. The integration in (13) cannot be expressed in terms of tabulated functions, and must be evaluated numerically.

12. Szabo, T.L., and Slobodnik, A.J., Jr. (1973) The effect of diffraction on the design of acoustic surface wave devices, IEEE Trans. SU-20:240-251.

While numerical integration is in general required to evaluate (13), simple analytic approximations can be obtained in the free surface case for large L. Using the approximation

$$\kappa \approx k_1 - \frac{\alpha_1^2}{2k_1}\eta_1^2 \tag{17}$$

it is seen that the exponential will go through rapid variations outside the range

$$0 \le \eta_1 \le \frac{2\pi}{\sqrt{\alpha_1^2 \lambda_1 L}} .$$

The rapid variations in turn result in cancellation for the portion of the integration interval outside of this range. If this range of η_1 lies within the central lobe $0 \le \eta_1 \le \pi/b$ of $(\sin \eta_1 b/\eta_1 b)^2$, then this function may be approximated by unity. The requirement that the upper limit of the range be less than π/b is equivalent to the far-field condition

$$F \equiv \left(\frac{L\alpha_1^2}{\lambda_1}\right) \Big/ \left(\frac{2b}{\lambda_1}\right)^2 > 1 \tag{18}$$

for transducers on a free surface.[12]

For a free surface $f(\eta_1) = 1$ so that using (17), D_L of (13) becomes

$$D_L \approx \frac{2b}{\pi} \int_0^\infty \exp\left[-i\left(\frac{\alpha_1^2}{2k_1} L\right) \eta_1^2\right] d\eta_1 = \frac{e^{-i\pi/4}}{\sqrt{F}} . \tag{19}$$

This expression gives the well known fact that diffraction loss varies as $1/\sqrt{L}$ for large L.

When the dc electrodes are present, it is not simple to approximate D_L. In Appendix C an approximation is derived for case a = b, when $k_1 b$ is large and $F \ge 3$. The approximation derived there gives

$$D_L \approx 2\left(\frac{2}{\pi}\right)^2 e^{-i\pi F/4} e^{-bF/B} + 4\left(\frac{2}{\pi}\right)^4 \frac{b}{B\sqrt{F}} e^{-i\pi/4} . \tag{20}$$

where

$$B = \frac{2}{\pi} b^2 \sqrt{k_2^2 - k_1^2}/\alpha_2 \quad .$$

As an example, ignoring mass loading effects of the electrodes, for 37-X $LiNbO_3$, $B/b = 1.23\ b/\lambda_1$, where λ_1 is the wavelength in the direction of propagation on the free surface. Then,

$$D_L \approx 0.811\, e^{-i\pi F/4}\, e^{-0.812(F\lambda_1/b)} + \frac{0.534\, e^{-i\pi/4}}{\sqrt{F\,(b/\lambda_1)}} \quad .$$

If $b = 10\lambda_1$ and $F \lesssim 50$, the term containing the exponential is larger than the algebraic term, and can even be larger than D_L for a free surface.

In order to understand the variation of D_L with the parameters F and b, we have numerically evaluated the integral in (13). The results are plotted in Figure 5, together with the diffraction loss for a free surface. For a narrow gap

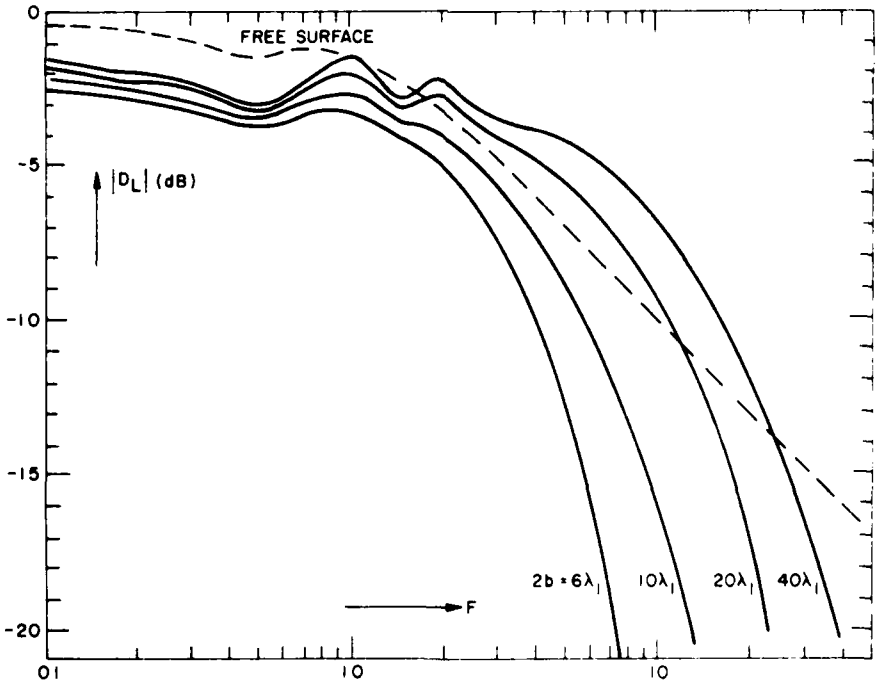

Figure 5. Variation of Diffraction Loss With Distance Parameter F for an Electrode Gap 2b

between the electrodes, the diffraction loss is greater than for a free surface, and it increases rapidly for F greater than about 5. For wide gaps, the diffraction loss can be less than the free surface loss over some range of F. However, for large F the diffraction loss increases rapidly and becomes greater than the free surface loss.

Application of the in-plane field configuration requires narrow gaps 2b for voltage sensitivity and long paths of propagation L to achieve large changes in time delay. For this choice of parameters, the use of wide electrodes leads to an increase in diffraction loss over that of a free surface. In the next section we consider methods for reducing diffraction loss.

4. REDUCTION OF DIFFRACTION LOSS FOR THE IN-PLANE CONFIGURATION

The measurements of Budreau, et al[3] indicate that for the high coupling cuts of $LiNbO_3$, the in-plane configuration suffers from low sensitivity of the velocity to applied electric field (V/m), as compared to the normal-field configuration. Since the dc bias electrodes can be made much closer for the in-plane configuration than for the normal-field case, the sensitivity to applied terminal voltage can be made higher. However, bringing the dc electrodes closer together has been seen to increase diffraction loss.

In this section we discuss modifications of the electrodes to reduce this loss. The first type of modification employs electrodes of narrow width w. The second employs surface platings in the region $|x| > b$ that stiffen the surface, thereby creating a slot waveguide in the region between the dc electrodes.

4.1 Narrow Electrodes

Wide electrodes, whose attenuation makes them appear to be semi-infinite, conduct energy away from the fields in the gap and thereby increase diffraction loss. One possible approach to reducing this loss is to use narrow electrodes to prevent the energy from being lost. Electrodes of finite width w act as $\Delta V/V_R$ waveguide. Thus, the field reaching the output transducer will be composed of modes guided by the electrodes, in addition to the unguided fields that are similar to the fields on the free surface of a crystal.

The reduction D_L in the output voltage due to diffraction loss can be separated into a component D_f representing the effect of the unguided field, and D_g representing the effect of the guided waves. Thus,

$$D_L = D_f + D_g \quad . \tag{21}$$

Expressions for D_f and D_g are derived in Appendix B. Neglecting dissipation of the guided waves by loss in the electrode platings, $|D_g|$ is independent of the separation L between the transducers, but decreases rapidly with separation 2a between the electrodes. On the other hand, D_f decreases with the ratio L/b^2.

The loss D_f due to the unguided fields is given by (13), with $f(\eta_1)$ replaced by (B7). Further manipulation of (B7) yields

$$f(\eta_1) \quad \left\{ \left[\cos \eta_2 w \sin \eta_1 a + (\eta_2/\eta_1) \sin \eta_2 w \cos \eta_1 a \right]^2 + \left[\cos \eta_2 w \cos \eta_1 a - (\eta_1/\eta_2) \sin \eta_2 w \sin \eta_1 a \right]^2 \right\}^{-1} \quad . \tag{22}$$

The functional dependence of $f(\eta_1)$ is sufficiently complex that it is not easily seen how to choose w to optimize D_f. For the case when $w = 0$, or the case when $k_1 = k_2$ and $\alpha_1 = \alpha_2$ so that $\eta_2 = \eta_1$, it is easily established that $f(\eta_1) = 1$, which is the value for a free surface. The free surface condition may be approximated for finite w if it is chosen such that

$$w\eta_2(0) = w \sqrt{k_2^2 - k_1^2}/\alpha_1 = \pi \quad . \tag{23}$$

Using such half-wave electrodes, $f(0) = 1$.

4.1.1 HALF-WAVE ELECTRODES

To evaluate the diffraction loss for electrodes of width w satisfying (23), we observe that the principle contribution to (13) comes from the interval $0 \le \eta_1 \le \pi/b$, where $\pi/b \ll \sqrt{k_2^2 - k_1^2}/\alpha_1$. Thus, we may use an approximation for $f(\eta_1)$. To develop the approximation we make use of

$$\eta_2 \approx \frac{1}{\alpha_2} \sqrt{k_2^2 - k_1^2} + \frac{\left(\alpha_1^2/\alpha_2\right)\eta_1^2}{2\sqrt{k_2^2 - k_1^2}} = \eta_2(0) + \frac{\alpha_1^2/\alpha_2^2}{2\eta_2(0)} \eta_1^2 \quad . \tag{24}$$

For w satisfying (23), to order η_1^2

$$\cos \eta_2 w \approx 1$$

$$\sin \eta_2 w \approx -w \frac{\alpha_1^2/\alpha_2^2}{2\eta_2(0)} \eta_1^2 \quad . \tag{25}$$

Using (24) and (25) in (22), we find that

$$f(\eta_1) = \left\{ \left[\sin \eta_1 a - \frac{w}{2} \left(\alpha_1^2/\alpha_2^2 \right) \eta_1 \cos \eta_1 a + O(\eta_1^3) \right]^2 + \left[\cos \eta_1 a + O(\eta_1^3) \right]^2 \right\}^{-1} . \tag{26}$$

In (26) we have not approximated $\sin \eta_1 a$ or $\cos \eta_1 a$ since for $a \gg \lambda_1$, they can vary significantly over the range of η_1 giving the primary contribution to (13).

Neglecting powers of η_1 greater than the first

$$f(\eta_1) \approx 1 + w \left(\alpha_1^2/\alpha_2^2 \right) \eta_1 \sin \eta_1 a \cos \eta_1 a . \tag{27}$$

When this expression for $f(\eta_1)$ is substituted into (13), the first term in (27) gives the diffraction loss for a pair of transducers on a free surface. The second term in (27) gives a correction that is small since the integrand varies as η_1^2 for η_1 small. Thus, the presence of the electrodes will result in only a small change in the diffraction loss over that of a free surface.

When the far-field condition (18) is satisfied, (13) can be approximated in closed form. In this case, the range of η_1 giving the primary contribution to the integral is determined by the exponent, rather than $(\sin \eta_1 b/\eta_1 b)^2$. Thus, we may approximate $\sin \eta_1 a \approx \eta_1 a$ and $\cos \eta_1 a \approx 1$. With these approximations and the help of (17) we have for a = b

$$D_f = \frac{e^{-i\pi/4}}{\sqrt{F}} \left[1 - i \frac{w}{b} \frac{\alpha_1^2}{\alpha_2^2} \frac{\pi}{2F} \right] . \tag{28}$$

For b large compared to w, the correction term in (28) will have only a small effect on $|D_L|$.

When w satisfies (23), the n = 1 mode is at cutoff, and hence gives vanishing contribution to (B20). Thus we need keep only the n = 0 mode in (B20) and obtain

$$D_g = \frac{4bk_1}{\kappa} \left(\frac{\sinh y_o b}{y_o b} \right)^2 \frac{y_o e^{-2y_o a} e^{i(\kappa - k_1)L}}{\left(1 + \frac{\alpha_1^2}{\alpha_2^2} \frac{y_o^2}{n_2^2} \right) - \frac{y_o w}{2} \frac{\alpha_1^2}{\alpha_2^2} \left(1 + \frac{y_o^2}{n_2^2} \right)} , \tag{29}$$

where γ_o is the decay constant along x of the guided wave fields in the free surface region, and η_2 and κ are found from (15) with $\eta_1 = j\gamma_o$.

To estimate the size of $|D_g|$ relative to $|D_f|$, we make use of the computations of Reference 8 for waveguides on Y - Z $LiNbO_3$. Assuming $b \gg a$ and that $\gamma_o b \geq 2$, it is found that

$$|D_g| \approx 1.22(\lambda_1 b) \quad 0.869\ (\gamma_o b) \quad .$$

If wide transducers are used so that $F \sim 1$, then $\lambda_1 \ll b$ and $|D_g| \ll |D_f|$. For this case the guided wave gives only a small contribution to the output voltage. The guided wave may result in some amplitude and phase ripple with frequency, since its propagation constant $\kappa(j\gamma_o)$ is different from k_1.

4.1.2 OTHER ELECTRODE WIDTHS

Electrodes that are an integer multiple of the width given by (23) will also lead to approximations for $f(\eta_1)$ similar to (27). The presence of such electrodes will therefore only slightly perturb D_f from its value for a free surface. However, such electrodes will have more modes above cutoff, thereby complicating the phase and amplitude dependence of D_g with frequency.

The half-wave electrodes result in less diffraction loss because they are, to first order, invisible to a SAW propagating along the z axis. One is led to speculate that an improvement in the loss could be achieved if the electrodes reflected the SAW back into the gap between the electrodes. Quarter-wave electrodes, having width half that given by (23), would have the largest reflection coefficient. Unfortunately, the reflection coefficient is negative, as can be seen from (B3) for $\eta_1 = 0$ and $\eta_2 w = \pi/2$ so that reflected waves add destructively with those still propagating in the gap. This result can also be seen from $f(\eta_1)$ in (22). If $\eta_2(0)w = \pi/2$, then $\cos \eta_2 w \approx 0$, $\sin \eta_2 w \approx 1$ and for η_1 small

$$f(\eta_1) \approx \frac{-\eta_1}{\eta_2(0) \cos \eta_1 a} \quad .$$

Because $f(\eta_1)$ depends linearly on η_1, the integral in (13) is smaller than it would be for a free surface.

4.2 Slot Waveguides

One way to achieve a narrow gap between electrodes, without increasing the diffraction loss is to plate the electrodes of Figure 2 with a material such as Al N

that stiffens the surface.[13] If the SAW velocity is thereby increased over the free surface SAW velocity, the gap region will act as a waveguide.[4, 5]

If the electrode consists of a very thin metallization, then the mechanical perturbation of the surface will be due only to the film used to stiffen the surface. To first order for thin platings, the electrical shorting and mechanical loadings are additive effects. Thus, for thin platings of hexagonal material, such as AlN, with C axis normal to the surface, the wave number k_2 under the plating is[6]

$$\frac{k_2 - k_1}{k_1} = \frac{\Delta V}{V_1} + \frac{V_1 h}{4P}\left[\left(\rho' - \frac{1}{V_1^2 s_{66}}\right)|v_x|^2 + \rho'|v_y|^2 + \left(\rho' - \frac{1}{V_1^2}\frac{s_{11}}{s_{11}^2 - s_{12}^2}\right)|v_z|^2\right] . \quad (30)$$

Here, V_1 is the SAW velocity along z on a free surface, and ΔV V_1 is the velocity change due to shorting of the piezoelectric fields. The plating material has thickness h, mass density ρ', and elastic stiffness constants s_{ij} in the coordinate system, where Z is along the C axis. Finally, v_x, v_y, and v_z are the particle velocity components at the surface $y = 0$ of a SAW carrying power along z of P Watts per meter.

Reference 14 lists the compliances C_{ij} for AlN. If these are used to obtain the s_{ij} elements as if the material were non-piezoelectric, then $1/s_{66} = 1.10 \times 10^{11}\ (N/m^2)$ and $s_{11}\ (s_{11}^2 - s_{12}^2) = 1.35 \times 10^{11}\ (N/m^2)$. Also, $\rho = 3.26 \times 10^3\ K_g/m^3$ so that for the 37-X cut of $LiNbO_3$ Expression (30) becomes

$$\frac{k_2 - k_1}{k_1} = 0.0268 - 0.222\ h/\lambda_1 . \quad (31)$$

It is seen that a layer of thickness $h \approx 0.12\lambda_1$ is necessary to overcome the slowing resulting from shorting of the electric field. The first order perturbation theory leading to (31) may not be accurate for films of this thickness, and a more accurate computer calculation is required to establish the actual value of h needed to overcome the slowing due to the conducting film.

---

13. Carr, P., Private conversation.

14. Tsubouchi, K., Sugari, K., and Mikoshiba, N. (1982) Zero temperature coefficient surface-acoustic-wave devices using epitaxial AlN films, Proc. 1982 Ultrasonics Symp., pp. 340-345.

For thicker platings, the SAW velocity $V_2 = \omega/k_2$ will be greater than the free surface velocity V_1. The highest SAW velocity possible is limited by the velocity of the shear wave propagating parallel to the surface. Platings that are thick enough to raise the SAW velocity above the shear wave velocity will cause the SAW to leak energy into the bulk of the crystal. The slowest of the two shear waves propagating along x in $LiNbO_3$ has velocity that is 1.022 times Rayleigh velocity on the 37-X cut. Therefore, $(k_2 - k_1)/k_1 = -0.022$ for the SAW under the plating to be a bound wave.

The condition necessary for guidance of a wave by a slot waveguide is that k_2 lie between the shear wave number and k_1. When this condition is satisfied, the wave numbers κ_n of the propagating waveguide modes lie between k_1 and k_2, so that η_2 is imaginary and η_1 is real. The dispersion relation for the guided waves of even symmetry about the centerline $x = 0$ is

$$\eta_2 = i\eta_1 \tan \eta_1 b \tag{32}$$

where η_1 and η_2 are related to κ_n via (A6). Equation (32) may be solved graphically for η_1 using the construction of Figure B1 with subscripts 1 and 2 interchanged and 2b used for w. Because the transducers are symmetric about the centerline, only the symmetric ($n = 0, 2, 4 \ldots$) modes need be considered.

The dispersion of slot waveguide modes is discussed in Reference 4 for the case of dielectric layers on anisotropic substrates. The presence of the shorting layer will modify somewhat the dispersion. In any case, the phase velocity $V_n = \omega/\kappa_n$ of the guided waves must lie between V_1 and V_2. Since V_2 must be less than the shear wave velocity, the difference between V_n and V_1 can be no more than a few percent. As a result, mode dispersion will not be a significant factor in the application of gap guides to phase shifters for phased array radar. If two or more modes can propagate, differences in their phase velocities may, however, produce undesirable amplitude variations with frequency.

The output voltage in the presence of the guide can be obtained by modifying the analysis of Appendix A. In Expression (A14), the poles of the integrand are those of the factor

$$\frac{1 + \Gamma e^{i2\eta_1 a}}{1 - \Gamma e^{i2\eta_1 a}} = \frac{\eta_1 - i\eta_2 \tan \eta_1 a}{\eta_2 - i\eta_1 \tan \eta_1 a} \quad . \tag{33}$$

It is seen from (33) that the poles occur at the roots of the dispersion relation, Eq. (32), for the guided waves. Referring to Figure A2, the poles associated

with the modes propagating in the positive z direction are located along the real κ axis to the right of the branch point k_2.

When the integration path is deformed around the branch cut through k_2, these poles are captured. The output voltage due to the poles is therefore

$$V_o \quad 2Q \frac{b^2}{\alpha_1^2} \sum_n \left(\frac{\sin \eta_1 b}{\eta_1 b} \right)^2 \frac{\eta_1 - i\eta_2 \tan \eta_1 a}{\frac{d}{d\kappa}(\eta_2 - i\eta_1 \tan \eta_1 a)} \frac{e^{i\kappa_n L}}{\eta_1} \quad . \tag{34}$$

where the sum is taken over the propagating modes and η_1 and η_2 are evaluated at the modal wavenumber κ_n. Making use of (15) and Eq. (32), and normalizing (34) by the Factor (B9), the contribution to the diffraction loss from the guided waves is found to be

$$D_g \quad 2 \sum_n \left(\frac{\sin \eta_1 b}{\eta_1 b} \right)^2 \frac{k_1}{\kappa_n} \frac{\eta_2 b \, e^{i(\kappa_n - k_1)L}}{\eta_2 a + i\left(\frac{\alpha_1^2}{\alpha_2^2} \cos^2 \eta_1 a + \sin^2 \eta_1 a \right)} \quad . \tag{35}$$

The contribution to the output voltage from the continuous spectrum is represented by the integration around the branch cut originating from k_2 in the κ plane. Because of the factor $(\sin \eta_1 b/\eta_1 b)^2$, the contribution from the continuous spectrum will be small if at $\kappa = k_2$, $\eta_1 b > \pi$. With the help of (A6) this condition is

$$b \sqrt{k_1^2 - k_2^2}/\alpha_1 > \pi \quad . \tag{36}$$

Alternatively, for F large, phase cancellation due to the exponential term will make the contribution from the continuous spectrum small. We do not consider this contribution further.

Condition (36) also implies that two or more modes of the slot guide are propagating. As an example, suppose that k_2 is 1 percent smaller than k_1. Using $\alpha_1 = 0.892$ for 37-X $LiNbO_3$.

$$b \sqrt{k_1^2 - k_2^2}/\alpha_1 = (0.317)\pi b/\lambda_1 \quad .$$

A gap 2b slightly larger than $6\lambda_1$ will satisfy (36).

To estimate D_g of (35) let $a = b$, $\alpha_1 = \alpha_2$ and assume that $b \sqrt{k_1^2 - k_2^2}/\alpha_1 = \pi$. Under these conditions the second mode will be at cutoff with $\eta_2 = 0$, and hence

will give a zero contribution to (35). With the approximation $\eta_1 b \approx \pi/2$ for the lowest mode gives with the help of (15)

$$\eta_2 b = i\frac{\alpha_1}{\alpha_2}\sqrt{\frac{b^2}{\alpha_1^2}\left(k_1^2 - k_2^2\right) - \eta_1^2 b^2} = i\pi\frac{\sqrt{3}}{2} \quad .$$

The n = 0 term in (35) then gives

$$|D_g| \approx 2\left(\frac{2}{\pi}\right)^2 \frac{\pi\sqrt{3}/2}{\pi\sqrt{3}/2 + 1} = 0.59 \quad ,$$

corresponding to -4.5 dB loss independent of L. For comparison, consider electrodes that are not stiffened. If $2b = 6\lambda_1$ and $\alpha_1^2 L/\lambda_1$ is 250 or greater, then $F \gtrsim 7$ and the diffraction loss is more than 25 dB. Thus, a substantial reduction in diffraction loss can be achieved for narrow dc electrode spacings by plating over the electrodes with a material that stiffens the surface.

5. RECOMMENDATIONS

In order to compare the various electrode configuration, we consider 1-GHz SAW devices on 38-X cut $LiNbO_3$. This cut was found to give the highest voltage sensitivity for both the normal-field and in-plane configurations.[3] For the normal-field case, an applied field of 1 MV/m gives a velocity change $\Delta V/V_R = 1.5 \times 10^{-4}$ in an L = 1.4 cm path. For the in-plane case $\Delta V/V_R = 6.2 \times 10^{-6}$ for $V_{DC}/2a = 1$ MV/m.

Based on the foregoing values, we have computed the dc voltage necessary to produce a change in delay of 1/2 an rf cycle (180° phase shift) at the output transducer. These values are listed in Table 1 for a 1-GHz SAW. For the raised electrode, the factor (5) was used in computing V_{DC}.

Propagation loss is also listed in the table. For a plated electrode in the normal-field configuration, the loss over free surface attenuation is due to loss in the film. The transducers are assumed wide enough to make diffraction loss negligible. For the in-plane configuration, loss represents the asymptotic forms of D_L valid for transducers that are short enough so that F > 1. In the case of slot waveguide, the loss represents mode coupling, which depends on 2b, but is independent of L. The value -5 dB is for $2b = 6\lambda_1 \approx 24\ \mu m$.

It is seen from Table 1 that relatively long paths are required to achieve 1/2-cycle delay changes with dc voltages under 100V. Propagation loss will be significant in all configurations. Using slot waveguides gives the lowest attenuation.

The foregoing conclusion suggests that slot guide deserves further consideration as a basis for phase shift devices. It is important to determine the effect of losses in the metal film and $A\ell N$ plating on the guided wave attenuation. A more rigorous theory must be employed to compute dispersion for SAW propagation under the plating, including the effects of finite metal thickness and the piezoelectric properties of $A\ell N$. When computing the dispersion of modes in the slot waveguide, it may also be necessary to account for effects at the edge of the plating, which are known to be important for gratings. Finally, the use of narrow electrodes may reduce loss and improve confinement. Criteria for determining the width of the narrow electrodes, and their location with respect to the edge of the $A\ell N$ plating, should be developed.

Table 1. Attenuation and Voltage Sensitivity for 1-GHz SAW on the 38-X Cut of $LiNbO_3$

	Propagation Loss Over Free Surface Attenuation of -2.5L dB	V_{DC} for 1/2-Cycle Delay Change
Normal field configuration* (250-μm thick plate, wide transducers):		
plated electrode (H = 0)	-7L dB	466/L
raised electrode (H = 5 μm)	0	1,260/L
In-plane configuration* (2a = 2b several wavelengths):*		
wide electrodes	$-1.8-1.79\times10^{6}\ L/(2b)^{3}$ dB	$45\left(\frac{2b}{L}\right)$
half-wave electrodes	$-45+20\log_{10}(2b)$ $-10\log_{10} L$ dB	
lowest mode of slot waveguide	~ -5 dB	

*Path length L is measured in cm, gap width 2b is measured in μm.

References

1. Joshi, S.G., and Dasgupta, B.B. (1981) Electronically variable surface acoustic wave time delay using a biasing electric field, Proc. 1981 IEEE Ultrasonics Symp., pp. 319-323.
2. Joshi, S.G. (1982) A temperature compensated high voltage probe using surface acoustic waves, Proc. 1982 IEEE Ultrasonics Symp., pp. 317-320.
3. Budreau, A.J., Carr, P.H., and Silva, J.H. (1982) New configuration for electronically variable SAW delay line, Proc. 1982 IEEE Ultrasonics Symp., pp. 399-400.
4. Schmidt, R.U., and Coldren, L.A. (1975) Thin film acoustic surface waveguides on anisotropic media, IEEE Trans. SU-22:115-122.
5. Tiersten, H.F. (1969) Elastic surface waves guided by thin films, J. Appl. Phys. 40:770-789.
6. Auld, B.A. (1973) Acoustic Fields and Waves in Solids, Vol. II, Wiley and Sons, New York, pp. 274-278.
7. Davis, K.L., and Weller, J.F. (1979) SAW attenuation in metal film - coated delay lines, Proc. 1979 IEEE Ultrasonics Symp., pp. 659-662.
8. Slobodnik, A.J., Jr., Carr, P.H., and Budreau, A.J. (1970) Microwave frequency acoustic surface-wave loss mechanisms on $LiNbO_3$, J. Appl. Phys. 41:4380-4387.
9. Snider, D.R., Fredricksen, H.P., and Schneider, S.C. (1981) Surface acoustic wave attenuation by a thin film, J. Appl. Phys. 52:3215-3222.
10. Durand, E. (1953) Electrostatique et Magnetostatique, Masson, Paris, pp. 302-303.
11. Budreau, A.J., Carr, P.H., and Bertoni, H.L. (1983) Highest sensitivity electrically variable SAW delay line, Proc. 1983 IEEE Ultrasonics Symp.
12. Szabo, T.L., and Slobodnik, A.J., Jr. (1973) The effect of diffraction on the design of acoustic surface wave devices, IEEE Trans. SU-20:240-251.
13. Carr, P., Private conversation.

14. Tsubouchi, K., Sugari, K., and Mikoshiba, N. (1982) Zero temperature coefficient surface-acoustic-wave devices using epitaxial A*l*N films, Proc. 1982 Ultrasonics Symp., pp. 340-345.

Appendix A

Diffraction Loss Due to DC Electrodes

In order to compute the diffraction loss due to the dc electrodes in Figure 2 we assume them to be semi-infinite in x and infinite in z. For wide electrodes that are slightly lossy, as is typically the case, the foregoing assumptions allow us to accurately model the diffraction loss in the simplest possible structure. The resulting geometry is shown in Figure A1. The electrode separation 2a is assumed to be greater than or equal to the transducer aperture 2b. Finally, the SAW velocity in the plated region 2 is assumed to be slightly smaller than that of the free surface region 1.

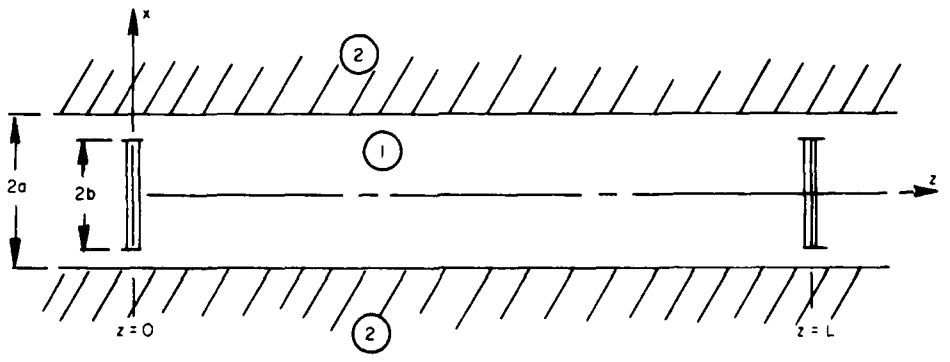

Figure A1. Configuration for Computing Diffraction Loss Due to Electrodes

Previous studies[A1] have shown that the SAW amplitude can be described by a potential function $\Psi(x, z)$. For crystal cuts, such as 37 - X $LiNbO_3$, that satisfy the parabolic approximation, energy from the sources the potential function in regions j = 1, 2 satisfies the wave equation

$$\left(\alpha_j^2 \frac{\partial^2}{\partial x^2} + \frac{\partial^2}{\partial z^2} + k_j^2\right) \Psi(x, z) = 0 \quad . \tag{A1}$$

Here k_j is the wave number of the SAW propagating in the z direction and α_j is related to the anisotropy parameter $\gamma = d^2V(\theta)/d\theta^2$ of Reference A2 via

$$\alpha_j^2 = 1 + \gamma_j \quad . \tag{A2}$$

Note that we are concerned with waves propagating primarily along z, with only a small x variation, so that the parabolic approximation is appropriate.

To find the SAW generated by the transducer, we represent the transducer by a collection of point sources $\delta(x - x')\delta(z)$ along the interval $-b < x' < b$. For each point source the potential $\Psi_g(x, z, x')$ must satisfy

$$\left(\alpha_j^2 \frac{\partial^2}{\partial x^2} + \frac{\partial^2}{\partial z^2} + k_j^2\right) \Psi_g = \delta(x - x')\, \delta(z) \quad . \tag{A3}$$

If we further employ a Fourier integral representation along z, then for time dependence $\exp(-i\omega t)$,

$$\Psi_g(x, z, x') = \frac{1}{2\pi} \int_{-\infty}^{\infty} \Phi(x, x', \kappa)\, e^{i\kappa z}\, d\kappa \quad . \tag{A4}$$

The transform $\Phi(x, x', \kappa)$ satisfies the equation

$$\left[\alpha_j^2 \frac{\partial^2}{\partial x^2} + \left(k_j^2 - \kappa^2\right)\right] \Phi = \delta(x - x') \quad . \tag{A5}$$

A1. Schmidt, R.V., and Coldren, L.A. (1975) Thin film acoustic surface waveguides on anisotropic media, IEEE Trans. SU-22:115-122.

A2. Slobodnik, A.J., Jr., Carr, P.H., and Budreau, A.J. (1970) Microwave frequency acoustic surface-wave loss mechanisms on $LiNbO_3$, J. Appl. Phys. 41:4380-4387.

The solution to Eq. (A5) can be constructed in terms of exponential solutions $\exp(\pm i\eta_j x)$, where

$$\eta_j = \frac{1}{\alpha_j} \sqrt{k_j^2 - \kappa^2} \quad . \tag{A6}$$

At the boundaries $x = \pm a$ we require that Φ and its normal derivative be continuous.[A1] As a result, the boundaries can be described by the reflection coefficient

$$\Gamma = \frac{\eta_1 - \eta_2}{\eta_1 + \eta_2} \quad . \tag{A7}$$

Thus, for $a > x > x'$

$$\Phi = A\left[e^{i\eta_1(x-a)} + \Gamma\, e^{-i\eta_1(x-a)}\right] \quad , \tag{A8}$$

while for $-a < x < x'$

$$\Phi = B\left[e^{-i\eta_1(x+a)} + \Gamma\, e^{i\eta_1(x+a)}\right] \quad . \tag{A9}$$

To find the coefficients A and B we return to Eq. (A5), which implies that Φ is continuous at $x = x'$, but that $\partial\Phi/\partial x$ jumps by $1/\alpha_1^2$. Using these conditions and solving for A and B gives

$$\Phi = \frac{1}{i2\alpha_1^2\eta_1 D}\left\{e^{i\eta_1|x-x'|}\, e^{-i\eta_1 a} + 2\Gamma\cos\left[\eta_1(x+x')\right]\right.$$

$$\left. + \Gamma^2\, e^{-i\eta_1|x-x'|}\, e^{i2\eta_1 a}\right\} \quad , \tag{A10}$$

where

$$D = e^{-i2\eta_1 a} - \Gamma^2\, e^{i2\eta_1 a} \quad . \tag{A11}$$

Substituting this expression into (A4) gives $\Psi_g(x, z; x')$.

To find the field at the output transducer it is necessary to integrate $\Psi_g(x, z;x')$ over the aperture $-b < x' < b$. The output voltage is then found by integrating the field over the output transducer $-b < x < b$. Thus, the output voltage is

$$V_0 = Q \int_{-b}^{b} \int_{-b}^{b} \Psi_g(x, L;x')\, dx\, dx' \quad , \tag{A12}$$

where Q is some constant of proportionality. Interchanging the order of integration over x', x with that of the integration over κ allows us to write

$$V_0 = \frac{Q}{2\pi} \int_{-\infty}^{\infty} \left[\int_{-b}^{b} \int_{-b}^{b} \Phi(x, x', \kappa)\, dx\, dx' \right] e^{i\kappa L}\, d\kappa \quad . \tag{A13}$$

Substituting from (A10) for $\Phi(x, x';\kappa)$ and carrying out the integrations over x' and x, one obtains, after some manipulation

$$V_0 = \frac{Q}{i\pi\alpha_1^2} \int_{-\infty}^{\infty} \left\{ \left[\left(\frac{\sin \eta_1 b}{\eta_1 b} \right)^2 \frac{1 + \Gamma e^{i2\eta_1 a}}{1 - \Gamma e^{i2\eta_1 a}} \right] - i \left[\frac{\sin 2\eta_1 b}{2\eta_1^2} - \frac{b}{\eta_1} \right] \right\} \frac{e^{i\kappa L}}{\eta_1}\, d\kappa \quad . \tag{A14}$$

Since for η_1 small

$$i \left[\frac{\sin 2\eta_1 b}{2\eta_1^2} - \frac{b}{\eta_1} \right] \approx i\, \frac{2}{3}\, \eta_1 b^3 \tag{A15}$$

the only pole singularities of the integrant occur at the roots of

$$\left(1 - \Gamma e^{i2\eta_1 a} \right) = 0 \quad . \tag{A16}$$

Using (A7), it can be seen that the integrand in (A14) is independent of the sign of η_1, so that its only branch points occur at $\kappa = \pm k_2$, where $\eta_2 = 0$.

The branch points $\pm k_2$ in the complex κ - plane are indicated in Figure A2, together with the associated branch cuts. The integration path implied in (A14) is also indicated. With these cuts, Im $\eta_2 \geq 0$ on the top Riemann sheet, and Re $\eta_2 \geq 0$ along the portion of the integration path in the interval $-k_2 < \kappa < k_2$.

In addition, the branch points $\kappa = \pm k_1$ of the function η_1 are indicated in Figure A2, along with the associated branch cuts (shown dashed). These cuts are not needed to evaluate (A14), but will clarify the subsequent discussion.

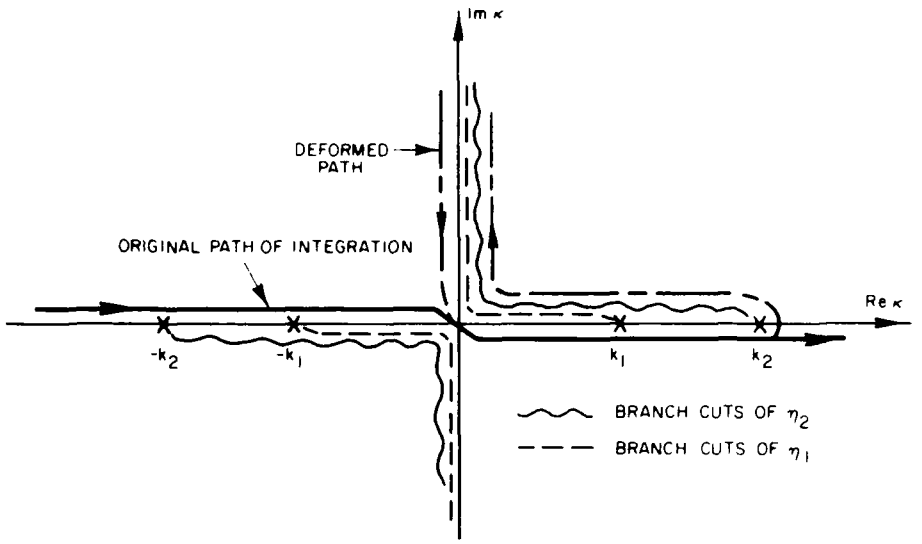

Figure A2. Integration Path in the Complex κ Plane

Taken together, the terms in the curved brackets of (A14) vanish for $|\kappa| \to \infty$. Thus, for $L > 0$, the integration path may be deformed into the upper half plane, as shown in Figure A2. For $k_2 > k_1$, the pole singularities of (A14) will be of the leaky wave type, and hence lie on the Riemann sheet for which Im $\eta_2 < 0$. Such poles are not intercepted during the deformation indicated in Figure A2.

Along the new path, η_1 is real and the terms in the square brackets of (A14) individually vanish as $\kappa \to i\infty$. Furthermore, the term

$$\left[\frac{\sin 2\eta_1 b}{2\eta_1^2} - \frac{b}{\eta_1}\right]\frac{e^{i\kappa L}}{\eta_1}$$

has the same value on both sides of the branch cut, so that its integration over the deformed path vanishes. Hence, we are left with only the first term in the square bracket of (A14).

Now make the change of variable to η_1 in the integration. Thus,

$$\kappa = \sqrt{k_1^2 - \alpha_1^2 \eta_1^2}$$

$$\eta_2 = \frac{1}{\alpha_2} \sqrt{\left(k_2^2 - k_1^2\right) + \alpha_1^2 \eta_1^2} \quad . \tag{A17}$$

With this change of variable, (A14) becomes

$$V_0 = \frac{Q}{i\pi} \int_{P_1} \left(\frac{\sin \eta_1 b}{\eta_1}\right)^2 \frac{1 + \Gamma e^{i2\eta_1 a}}{1 - \Gamma e^{i2\eta_1 a}} \frac{e^{i\kappa L}}{\kappa} d\eta_1 \quad , \tag{A18}$$

where the mapping of the integration path P_1 in the complex η_1-plane is shown in Figure A3. The branch points $\pm k_1/\alpha_1$ of κ are also shown, together with the branch points $\pm(i/\alpha_1)\sqrt{k_2^2 - k_1^2}$ of the function η_2 in (A17). With the choice of branch cut shown in Figure A3, η_2 has the same sign as η_1 along the real η_1 axis, which is consistent with the sign of η_2 along the deformed integration path in Figure A2. Note that for $k_2 = k_1$, this branch cut disappears. Also, $\Gamma = 0$ for this case and (A18) reduces to the diffraction integral for two uniform transducers on a free surface, as is to be expected.

To further simplify (A18), we use (A7) to show that

$$\frac{1 + \Gamma e^{i2\eta_1 a}}{1 - \Gamma e^{i2\eta_1 a}} = \frac{\eta_1 \eta_2 - i(\sin \eta_1 a)(\cos \eta_1 a)(\eta_2^2 - \eta_1^2)}{\eta_2^2 - \left(\eta_2^2 - \eta_1^2\right)\left(\sin \eta_1 a\right)^2} \quad . \tag{A19}$$

Along the real η_1 axis, the real port of (A19) is an even function while the imaginary part is odd. Thus, the contribution V_{OR} to (A18) from the real axis portion of the path P_1 is given by

$$V_{OR} = \frac{2Qb^2}{i\pi} \int_0^\infty \left\{ \left(\frac{\sin \eta_1 b}{\eta_1 b}\right)^2 \left[\frac{\eta_1 \eta_2}{\eta_2^2 - \left(\eta_2^2 - \eta_1^2\right)\left(\sin \eta_1 a\right)^2} \right] \right\} \frac{e^{i\kappa L}}{\kappa} \, d\eta_1 \quad . \tag{A20}$$

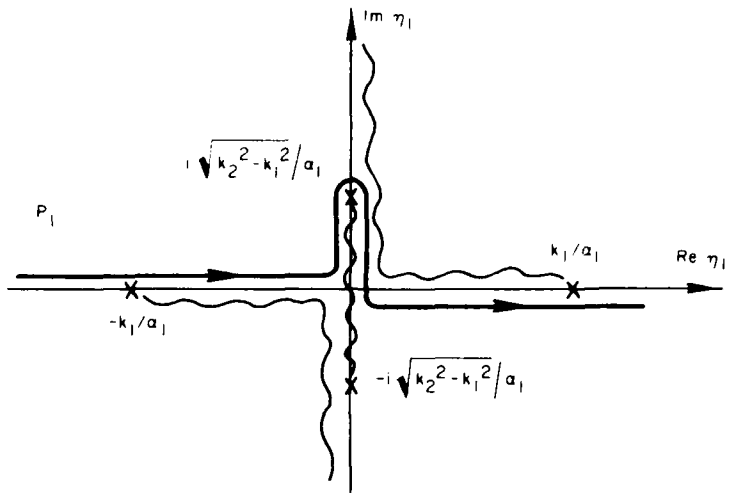

Figure A3. Integration Path in the Complex η Plane

For the portion of the integration path P_1 along the imaginary η_1 axis, let $\eta_1 = iy$ where $0 < y < (1/\alpha_1)\sqrt{k_2^2 - k_1^2}$. On the right-hand side of the branch cut η_2 is positive real, while on the left-hand side it is negative real. Substituting $\eta_1 = iy$ into (A19), and making use of the symmetry of η_2, the contribution V_{OI} to (A18) from the portion of the path along the imaginary axis can be written

$$V_{OI} = \frac{2Qb^2}{i\pi} \int_0^{\sqrt{k_2^2-k_1^2}/\alpha_1} \left\{ \left(\frac{\sinh yb}{yb}\right)^2 \frac{y\eta_2}{\eta_2^2 + \left(\eta_2^2 + y^2\right)(\sinh ya)^2} \right\} \frac{e^{ikL}}{\kappa}\, dy \quad , \tag{A21}$$

where from (A17)

$$\kappa = \sqrt{k_1^2 + \alpha_1^2 y^2}$$

$$\eta_2 = \frac{1}{\alpha_2}\sqrt{\left(k_2^2 - k_1^2\right) - \alpha_1^2 y^2} \quad . \tag{A22}$$

In order to understand the dependence of V_{OR} and V_{OI} on the parameters a and b we substitute Expressions (A17) and (A22) for η_2 and assume that $k_2^2 - k_1^2 \ll k_2^2$. The two factors in the curved brackets of (A20) are plotted in Figure A4 for the case $a, b \gg 2\pi\alpha_2 / \sqrt{k_2^2 - k_1^2}$. The plot of $(\sin \eta_1 b/\eta_1 b)^2$ is self explanatory. The plot of the second factor is obtained by approximating η_2 by $\sqrt{k_2^2 - k_1^2}/\alpha_2$ for η_1 small. Then, the square bracket term in (A20) for $\eta_1 \ll \sqrt{k_2^2 - k_1^2}/\alpha_1$ becomes

$$\left[\ \right] \approx \frac{\eta_1 \sqrt{k_2^2 - k_1^2}/\alpha_2}{\frac{k_2^2 - k_1^2}{\alpha_2^2} (\cos \eta_1 a)^2 + \eta_1^2 (\sin \eta_1 a)^2} \quad . \tag{A23}$$

which has maxima when $\eta_1 a$ is an odd multiple of $\pi/2$, and minima when $\eta_1 a$ is a multiple of π.

For $\eta_1 \gg \sqrt{k_2^2 - k_1^2}/\alpha_1$, it is seen that $\eta_2 \approx \alpha_1 \eta_1 / \alpha_2$ and the square bracket term in (A20) can be approximated as

$$\left[\ \right] \approx \frac{\alpha_2}{\alpha_1} \left\{ 1 - \frac{1}{2} \left[\left(\frac{\alpha_1^2}{\alpha_2^2} - 1 \right) + \frac{k_2^2 - k_1^2}{\alpha_2^2 \eta_1^2} \right] (1 - \cos 2\eta_1 a) \right\} \quad . \tag{A24}$$

Because α_1 is close to α_2, this factor is seen to have small oscillations about

$$\frac{\alpha_2}{\alpha_1} \left[1 - \frac{1}{2} \left(\frac{\alpha_1^2}{\alpha_2^2} - 1 \right) \right] \quad . \tag{A25}$$

For example, the 37-X cut of $LiNbO_3$ has $\alpha_1^2 = 0.795$ and $\alpha_2^2 = 0.687$ so that $(1/2)(\alpha_1^2/\alpha_2^2 - 1) = 0.079$ and (A25) has value 0.857.

When the electrode spacing 2a is large compared to the transducer aperture 2b, the period of oscillation π/a of the factor in (A23) or (A24) is small compared to the period of oscillation π/b of $(\sin \eta_1 b/\eta_1 b)^2$. These rapid oscillations will cancel in the integration of (A20), with the result that the integral is close to its value for $k_2 = k_1$. In other words, when $a \gg b$ the output voltage is close to that for transducers on a free surface.

For the case $a = b$, the product of the two factors of Figure A4 is sketched in Figure A5. For comparison, we have also sketched (dashed) in Figure A5 the term in the curved bracket of (A21) for the same case $a = b$. The area under the

dashed curve will be smaller than that under the solid curve by a factor proportional to the ratio of amplitudes of the two curves. This ratio is proportional to $\alpha_2^2 / \left[a^2 \left(k_2^2 - k_1^2 \right) \right]$. For the 37-X cut of LiN_bO_3, this factor is $(0.33)(\lambda_1/a)^2$. Thus, for a wide aperture ($a \gg \lambda_1$), the contribution V_{OI} of (A21) to the total output voltage V_o is small compared to V_{OR} of (A20).

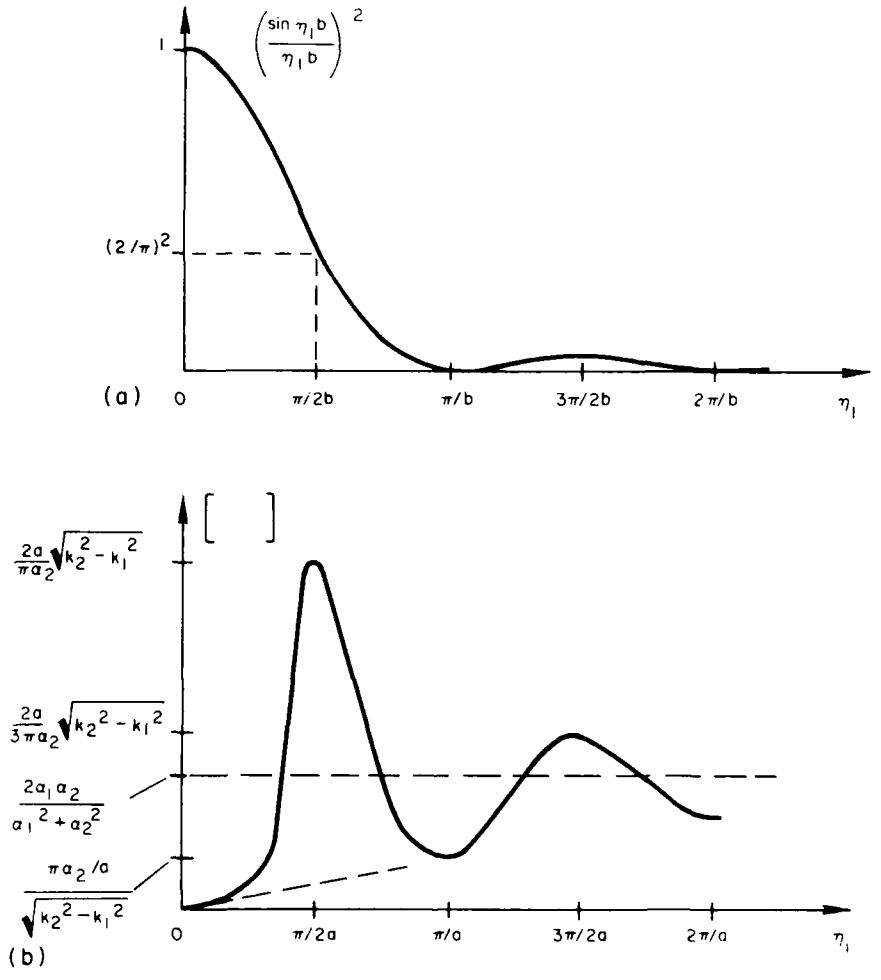

Figure A4. Variation of the Factors in the Integrand of V_{OR}

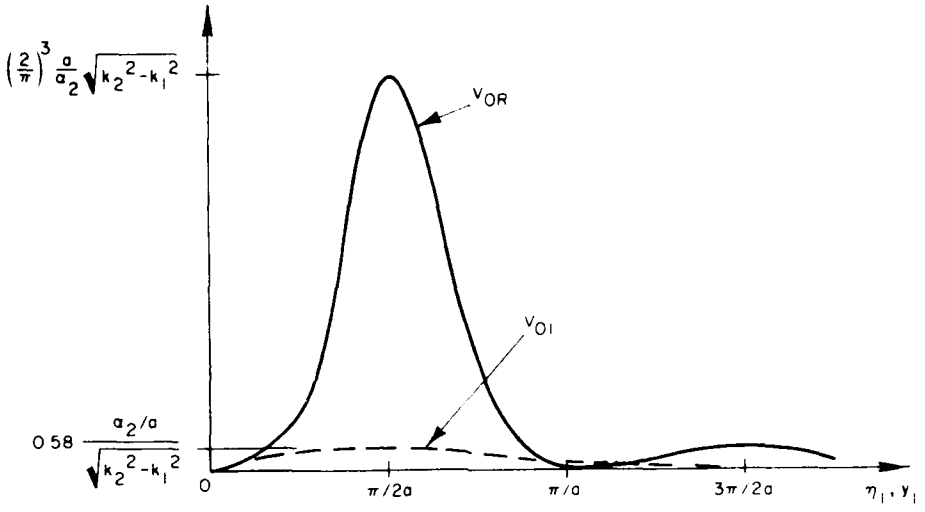

Figure A5. Comparison of the Integrands for V_{OR} and V_{OI}

Because the principal contribution to the integration in (A20) comes from $\eta_1 < 2\pi/b \ll k_1$, the factor $1/\kappa$ can be replaced by $1/k_1$. With the foregoing approximations, *the diffraction loss* D_L *due to the electrodes and/or due to path length* L is given by V_{OR} normalized to its value for L = 0 and $k_1 = k_2$. Thus,

$$D_L = \frac{2b}{\pi} \int_0^\infty \left(\frac{\sin \eta_1 b}{\eta_1 b}\right)^2 \left[\frac{\eta_1 \eta_2}{\eta_2^2 - \left(\eta_2^2 - \eta_1^2\right)(\sin \eta_1 a)^2}\right] e^{i(\kappa - k_1)L} \, d\eta_1 \quad . \tag{A26}$$

where we have made use of

$$\int_0^\infty \left(\frac{\sin \eta_1 b}{\eta_1 b}\right)^2 d(\eta_1 b) = \frac{\pi}{2} \quad . \tag{A27}$$

While (A26) was derived using the quadratic approximation for the dispersion curve, the approximation served primarily to make clear the location of branch points and branch cuts during the deformation of the integration path. However, the branch points occur explicitly in (A26) only via the definition of κ and η_2, and not in integration path. This result suggests that if numerically generated

dispersion curves were available for κ and α_2, (A26) could be used for materials for which the quadratic approximation is not valid.

To gain insight into (A26), we approximate D_L for large L and large a = b. When L is large, the exponential term undergoes rapid phase variation for $\eta_1 > \pi/b$, with the result that the contributions to the integral from neighboring segments of the η_1 axis cancel each other. However, the large first maximum of the function

$$f(\eta_1) \quad \frac{\eta_1 \eta_2}{\eta_2^2 - \left(\eta_2^2 - \eta_1^2\right)(\sin \eta_1 a)^2} \tag{A28}$$

evident in Figure A4(b) will significantly influence the value of the integral. The shape of the maximum suggests an approximation of the form

$$f(\eta_1) \approx \eta_1 \frac{(2a/\pi)^2 \sqrt{k_2^2 - k_1^2}/\alpha_2}{1 + B^2\left(\eta_1^2 - \pi/2a\right)^2} \quad , \tag{A29}$$

which gives the correct value of $f(\pi/2a)$. The coefficient B is found by requiring that the second derivative of the Approximation (A29) evaluated at $\pi/2a$ give the correct value for large a. This requirement leads to

$$B = \frac{2}{\pi} a^2 \sqrt{k_2^2 - k_1^2}/\alpha_2 \quad . \tag{A30}$$

The factor η_1 in (A29) cancels one power of η_1 in the factor $(\sin \eta_1 b/\eta_1 b)^2$ in (A26). The first two terms in the series expansion of $(\sin \eta_1 b/\eta_1)$ about $\pi/2b$ are

$$\frac{(\sin \eta_1 b)^2}{\eta_1} \approx b \frac{2}{\pi} \left[1 - \frac{2b}{\pi} \left(\eta_1 - \frac{\pi}{2b}\right)\right] \quad . \tag{A31}$$

With the help of (A29) and (A31), the integral in (A26) for a = b can be written

$$D_L = \left(\frac{2}{\pi}\right)^4 b^2 \frac{k_2^2 - k_1^2}{\alpha_2} \int_0^\infty \frac{(2 - \eta_1 2b/\pi)\, e^{i(\kappa - k_1)L}}{1 + B^2(\eta_1 - \pi/2b)^2} \, d\eta_1 \quad . \tag{A32}$$

Because of the large factor B in the denominator of (A32), the integrand will be small for $\eta_1 < 0$. Hence, we may extend the lower limit to $\eta_1 = -\infty$. If we now use the Approximation (17) for κ, and carry out a partial fraction expansion of the integrand, (A32) becomes

$$D_L = \frac{b}{i2}\left(\frac{2}{\pi}\right)^4 \left\{ \left(\frac{\pi}{2} - i\,\frac{b}{B}\right) \int_{-\infty}^{\infty} \frac{\exp[-i(F/\pi)(\eta_1 b)^2]}{\eta_1 b - (\pi/2 + ib/B)}\, d\eta_1 \right.$$

$$\left. - \left(\frac{\pi}{2} - i\,\frac{b}{B}\right) \int_{-\infty}^{\infty} \frac{\exp[-i(F/\pi)(\eta_1 b)^2]}{\eta_1 b - (\pi/2 - ib/B)}\, d\eta_1 \right\} , \qquad \text{(A33)}$$

where F is defined in (18). The integrals in (A33) can now be evaluated in closed form.

To evaluate the integrals in (A33), the paths of integration along the real η_1 axis are deformed into paths at 45° to the real axis starting in the second quadrant of the complex η_1 plane, and ending in the fourth quadrant. During the deformation, the pole at $(\pi/2 - ib/B)$ in the second integral is captured, giving rise to a residue contribution. The integrations along the slant path can be expressed in terms of the complementary error function. As a result of this evaluation one obtains[A3]

$$D_L = \frac{1}{i2}\left(\frac{2}{\pi}\right)^4 \left\{ 2\pi i\left(\frac{\pi}{2} + i\,\frac{b}{B}\right) \exp\left[-i\,\frac{F}{\pi}\left(\frac{\pi}{2} - i\,\frac{b}{B}\right)^2\right] \right.$$

$$+ \left(\frac{\pi}{2} - i\,\frac{b}{B}\right)(i\pi)\, e^{-T_+^2}\, \mathrm{erfc}(-iT_+)$$

$$\left. - \left(\frac{\pi}{2} + i\,\frac{b}{B}\right)(i\pi)\, e^{-T_-^2}\, \mathrm{erfc}(-iT_-) \right\} , \qquad \text{(A34)}$$

where

$$T_\pm = \sqrt{\frac{F}{\pi}}\left(\frac{\pi}{2} \pm i\,\frac{b}{B}\right) e^{i\pi/4} . \qquad \text{(A35)}$$

A3. Abramowitz, M., and Stegun, I. A. (1964) Handbook of Mathematical Functions, National Bureau of Standards, Washington, D. C., pp. 297-298.

From (A30), for a = b it is seen that b/B is proportional to 1/b, and hence for b large $b/B \ll \pi/2$. Also, for F large, $|T^{\pm}|$ will be large so that[A3]

$$e^{-T^2}\,\mathrm{erfc}(-iT) \sim \frac{i}{\sqrt{\pi}\,T} \quad . \tag{A36}$$

Using (A36) in (A34) and, after combining terms containing the complementary error function, neglecting b/B compared to $\pi/2$ in amplitude terms

$$D_L \sim 2\left(\frac{2}{\pi}\right)^2 e^{-i\pi F/4}\, e^{-bF/B} + 4\left(\frac{2}{\pi}\right)^4 \frac{b}{B\sqrt{F}}\, e^{-i\pi/4} \quad . \tag{A37}$$

The approximations leading to (A37) are valid for F greater than about 3. Since $b/B \ll \pi/2$, the first term in (A37) will be larger than the second for F less than about $(B/b)^2$.

Appendix B

Effects of Finite Width Electrodes

Electrodes of finite width w are shown in Figure 2. Consistent with the representation of the SAW amplitude in terms of a potential function, as discussed in Appendix A, the impedance looking in the x-direction for waves having variation exp (iκz) along z is $1/\eta_1$ in the free surface region, and $1/\eta_2$ in the plated region. Thus, the impedance seen at z = a looking into the finite width plating region can be found from the transmission line analogue for exp (-iωt) time dependence as

$$Z_{in} = \frac{1}{\eta_2} \frac{(1/\eta_1) - i(1/\eta_2) \tan \eta_2 w}{(1/\eta_2) - i(1/\eta_1) \tan \eta_2 w} \quad . \tag{B1}$$

The impedance (B1) reflects waves incident along x with reflection coefficient

$$\Gamma = \frac{Z_{in} - (1/\eta_1)}{Z_{in} + (1/\eta_1)} \quad . \tag{B2}$$

Substituting from (B1) we obtain

$$\Gamma = \frac{i\left(\eta_2^2 - \eta_1^2\right) \tan \eta_2 w}{2\eta_1\eta_2 - i\left(\eta_2^2 + \eta_1^2\right) \tan \eta_2 w} \quad . \tag{B3}$$

This expression for Γ may now be used in the integral Expression (A14) for the output voltage V_o.

The reflection coefficient appears in (A14) through the function

$$\hat{f}(\eta_1) = \frac{1 + \Gamma e^{i2\eta_1 a}}{1 - \Gamma e^{i2\eta_1 a}} . \tag{B4}$$

Substituting for Γ from (B3), and after suitable manipulation, it is found that

$$\hat{f}(\eta_1) = \frac{\left(1 - i\frac{\eta_1}{\eta_2}\tan \eta_2 \frac{w}{2}\right)\left(1 - i\frac{\eta_2}{\eta_1}\tan \eta_2 \frac{w}{2}\right) - i\left(\frac{\eta_1}{\eta_2} - \frac{\eta_2}{\eta_1}\right)\tan \eta_2 \frac{w}{2}\, e^{i2\eta_1 a}}{\left(1 - i\frac{\eta_1}{\eta_2}\tan \eta_2 \frac{w}{2}\right)\left(1 - i\frac{\eta_2}{\eta_1}\tan \eta_2 \frac{w}{2}\right) + i\left(\frac{\eta_1}{\eta_2} - \frac{\eta_2}{\eta_1}\right)\tan \eta_2 \frac{w}{2}\, e^{i2\eta_1 a}} . \tag{B5}$$

It is seen from (B5) that $\hat{f}$ is unchanged by changing the sign of η_2. Hence, the branch points at $\pm k_2$ in Figure A2 are not present in the integrand. However, the branch points at $\pm k_1$ are present in $\hat{f}$, reflecting the fact that the free-surface region extends to $|x| \to \infty$.

The function $\hat{f}$ will have one or more poles in the segment of the real κ axis between k_1 and k_2. In this segment η_2 is real and η_1 is positive imaginary. If the original path of integration is deformed as shown in Figure A2, then the portion of the path from k_1 to k_2 and back again to k_1 will enclose these poles. Changing the variable of integration to η_1 results in the path P_1 of Figure A3 for the integral of (A18). In the η_1 plane, the integration along the real axis gives the contribution from the continuous spectrum to V_o. The portion of P_1 from the origin to the point $i\sqrt{k_2^2 - k_1^2}/\alpha_1$ and back to the origin encompasses the poles of $\hat{f}$, and gives the contribution to V_o from the guided waves.

B1. CONTINUOUS SPECTRUM CONTRIBUTION

To compute the contribution from the continuous spectrum we note that $(\sin \eta_1 b/\eta_1 b)^2$ and κ are even functions of η_1. Thus, only the symmetric portion of $\hat{f}$ will survive the integration along the real η_1 axis. Define symmetric part $f(\eta_1)$ as

$$f(\eta_1) = \frac{1}{2}\left[\hat{f}(\eta_1) + \hat{f}(-\eta_1)\right] . \tag{B6}$$

Recalling that η_2 is odd function of η_1 along the Re η_1 axis and after suitable manipulation it can be shown that

$$f(\eta_1) = \left\{ (\cos \eta_2 w)^2 - \left(\frac{\eta_1}{\eta_2} - \frac{\eta_2}{\eta_1} \right) (\sin \eta_2 w)(\cos \eta_2 w)(\sin 2\eta_1 a) + \frac{1}{2} (\sin \eta_2 w)^2 \left[\left(\frac{\eta_1^2}{\eta_2^2} + \frac{\eta_2^2}{\eta_1^2} \right) - \left(\frac{\eta_1^2}{\eta_2^2} - \frac{\eta_2^2}{\eta_1^2} \right) \cos 2\eta_1 a \right] \right\}^{-1} . \quad \text{(B7)}$$

The output voltage V_{OR} due to the continuous spectrum is now given by (A20) with the term in the square bracket replaced by $f(\eta_1)$. Thus,

$$V_{OR} = \frac{2Qb^2}{i\pi} \int_0^\infty \left(\frac{\sin \eta_1 b}{\eta_1 b} \right)^2 f(\eta_1) \frac{e^{i\kappa L}}{\kappa} d\eta_1 . \quad \text{(B8)}$$

Dividing this expression by

$$\frac{2Qb^2}{i\pi} \left[\int_0^\infty \left(\frac{\sin \eta_1 b}{\eta_1 b} \right)^2 d\eta_1 \right] \frac{e^{ik_1 L}}{k_1} = \frac{Qb}{ik_1} e^{ik_1 L} \quad \text{(B9)}$$

normalizes V_{OR} to the output voltage when the two transducers are close together on a free surface. The normalized voltage is represented by the symbol D_f. Note that κ in the denominator of (B8) can be replaced by k_1 with little error for $b \gg \lambda_1$.

B2. GUIDED WAVE CONTRIBUTION

The guided waves decrease exponentially in amplitude for $|x| \to \infty$. This decay results from the fact that η_1 is imaginary at the pole. Substituting $\eta_1 = iy$ into the denominator of $\hat{f}$ in (B5), and equating it to zero, gives the dispersion equation of the guided waves as

$$\left(1 + \frac{y}{\eta_2} \tan \eta_2 \frac{w}{2}\right)\left(1 - \frac{\eta_2}{y} \tan \eta_2 \frac{w}{2}\right) - \left(\frac{y}{\eta_2} - \frac{\eta_2}{y}\right) \tan \eta_2 \frac{w}{2}\, e^{-2ya} = 0 \quad . \tag{B10}$$

The first term in (B10) gives the dispersion equation for an isolated strip, while the second term represents the perturbation due to coupling between the strips.[B1] If the strips are separated by several wavelengths, the coupling is small, and hence the guided wave solutions for the pair of strips will be close to the solutions for an isolated strip.

As a result of the coupling between strips, each mode of the isolated strip will split into two modes. One mode is symmetric with respect to the centerline $x = 0$, and the other is antisymmetric. For symmetric transducers, as is assumed here, only the symmetric mode is excited. Because $f(\eta_1)$ describes interactions in a symmetric structure, its poles are only those of guided waves having even symmetry about the centerline.

The modes of an isolated strip have either even or odd symmetry about the center of the strip. Even modes, including the lowest mode, are given mode index ($n = 0, 2, 4, \ldots$), and are solutions of the dispersion equation

$$y = \eta_2 \tan \eta_2 \frac{w}{2} \quad . \tag{B11}$$

The dispersion equation of the odd modes, having mode index ($n = 1, 3, 5, \ldots$), is

$$y = -\frac{\eta_2}{\tan \eta_2 \frac{w}{2}} \quad . \tag{B12}$$

Insight into these solutions is gained by solving (15) for $y = i\eta_1$ in terms of η_2 real. Thus,

$$y = \frac{1}{\alpha_1} \sqrt{\left(k_2^2 - k_1^2\right) - \alpha_2^2 \eta_2^2} \quad . \tag{B13}$$

B1. Schmidt, R. U., and Coldren, L. A. (1975) Thin film acoustic surface waveguides on anisotropic media, IEEE Trans. SU-22:115-122.

The solution to Eqs. (B11) or (B12) is then given by the intersection of the plot of the right-hand side of these equations with the plot of the right-hand side of (B13). Such plots are indicated in Figure B1. It is seen that one or more real solutions for η_2 exist depending on the size of $\sqrt{k_2^2 - k_1^2}/\alpha_2$ relative to π/w. The cutoff frequency for the nth mode is found from the condition

$$\frac{1}{\alpha_2}\sqrt{k_1^2 - k_2^2} = \frac{n\pi}{w} \quad . \tag{B14}$$

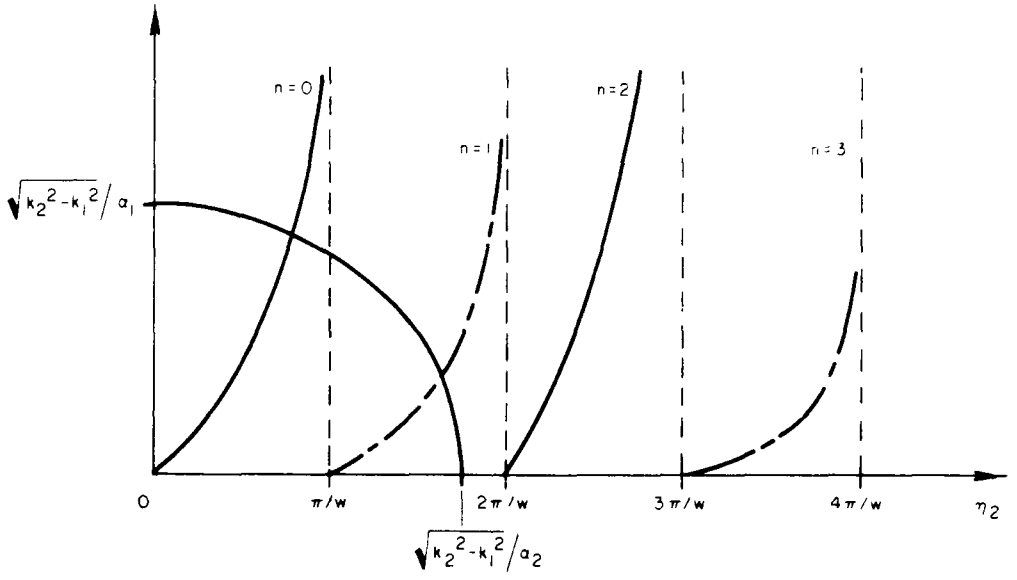

Figure B1. Construction for Finding the Solutions to the Dispersion Relation for an Isolated Strip

To find the voltage V_{OI} due to the guided modes let $\hat{N}(\eta_1)$ be the numerator of $\hat{f}(\eta_1)$ in (B5), and let $\hat{D}(\eta_1)$ be its denominator. Since the poles are encircled in the clockwise direction, then the residue contribution is

$$V_{OI} = -2Qb^2 \sum_{n=0,\,1,\,\ldots} \left[\left(\frac{\sin \eta_1 b}{\eta_1 b} \right)^2 \frac{\hat{N}(\eta_1)}{d\hat{D}(\eta_1)/d\eta_1} \frac{e^{i\kappa(\eta_1)L}}{\kappa(\eta_1)} \right]_{\eta_1 = iy_n} \quad . \tag{B15}$$

where iy_n is the location of the nth pole, and the sum is taken over the poles for which η_1 is pure imaginary, corresponding to propagating guided waves.

In order to evaluate (B15), we approximate the pole location by the solution of Eqs. (B11) or (B12) for an isolated strip. For the even modes we use (B10) and Eq. (B11) to obtain

$$\hat{N}(iy_n) = 2\left(\frac{y_n}{\eta_2} + \frac{\eta_2}{y_n}\right) \tan \eta_2 \frac{w}{2}\, e^{-2y_n a}$$

$$= 2\left(1 + y_n^2/\eta_2^2\right) e^{-2y_n a} \quad . \tag{B16}$$

For odd modes, (B10) and Eq. (B12) give

$$\hat{N}(iy_n) = -2\left(1 + \eta_2^2/y_n^2\right) e^{-2y_n a} \quad . \tag{B17}$$

For $2y_n a$ large, the derivative of the term containing the exponential in $D(\eta_1)$ will be small, when evaluated at $\eta_1 = iy_n$, as compared to the derivatives of the other term. Neglecting the exponential, it can be shown that at the even-numbered poles

$$\frac{d\hat{D}}{d\eta_1} = \left(1 - i\,\frac{\eta_1}{\eta_2} \tan \eta_2 \frac{w}{2}\right)\left[\frac{d}{d\eta_1}\left(-i\,\frac{\eta_2}{\eta_1} \tan \eta_2 \frac{w}{2}\right)\right] \quad , \tag{B18}$$

while at the odd-numbered poles

$$\frac{d\hat{D}}{d\eta_1} = \left[\frac{d}{d\eta_1}\left(-i\,\frac{\eta_1}{\eta_2} \tan \eta_2 \frac{w}{2}\right)\right]\left(1 - i\,\frac{\eta_2}{\eta_1} \tan \eta_2 \frac{w}{2}\right) \quad . \tag{B19}$$

Using the parabolic approximation (15) for $\eta_2(\eta_1)$ and Eqs. (B11) or (B12), the various terms in the residue series (B15) can be simplified. After some manipulation one finds that

$$V_{OI} = -4iQb^2 \sum_n \left(\frac{\sinh y_n b}{y_n b}\right)^2 \frac{y_n\, e^{-2y_n a}\, e^{ik(iy_n)L}/\kappa(iy_n)}{\left(1 + \frac{\alpha_1^2}{\alpha_2^2}\frac{y_n^2}{\eta_{2n}^2}\right) + \frac{y_n w}{2}\frac{\alpha_1^2}{\alpha_2^2}\left(1 + \frac{y_n^2}{\eta_{2n}^2}\right)} \quad . \tag{B20}$$

where the sum is taken over the propagating modes and η_{2n} is the value of η_2 at $\eta_1 = iy_n$. At cutoff for each mode $y_n = 0$, so that the contribution to (B20) from each mode initially increases from zero as frequency increases above its cutoff. Far enough from cutoff so that $2y_n a \geq 4$, $\sinh y_n b \approx (1/2)\, e^{y_n b}$, which simplifies the evaluation of (B20). Dividing (B20) by the Factor (B9) gives the normalized voltage that has been labeled D_g in Section 2.

MISSION
of
Rome Air Development Center

RADC plans and executes research, development, test and selected acquisition programs in support of Command, Control Communications and Intelligence (C^3I) activities. Technical and engineering support within areas of technical competence is provided to ESD Program Offices (POs) and other ESD elements. The principal technical mission areas are communications, electromagnetic guidance and control, surveillance of ground and aerospace objects, intelligence data collection and handling, information system technology, ionospheric propagation, solid state sciences, microwave physics and electronic reliability, maintainability and compatibility.

Printed by
United States Air Force
Hanscom AFB, Mass. 01731